UNCLASSIFIED

CONFIDENTIAL

Copy
RM L50D04

NACA RM L50D04

NACA
RM-L50D04

NACA
CASE FILE
COPY

GROUP 4
Downgraded at 3 year intervals; declassified after 12 years

RESEARCH MEMORANDUM

DETERMINATION BY THE FREE-FALL METHOD OF THE DRAG AND LONGITUDINAL STABILITY AND CONTROL CHARACTERISTICS OF A CANARD MODEL AT TRANSONIC SPEEDS

By Christopher C. Kraft, Jr. and Charles W. Mathews

Langley Aeronautical Laboratory
Langley Air Force Base, Va.

CASE FILE
COPY

JPL LIBRARY
CALIFORNIA INSTITUTE OF TECHNOLOGY

CLASSIFIED DOCUMENT

This document contains classified information affecting the National Defense of the United States within the meaning of the Espionage Act, USC 50:31 and 32. Its transmission or the revelation of its contents in any manner to an unauthorized person is prohibited by law. Information so classified may be imparted only to persons in the military and naval services of the United States, appropriate civilian officers and employees of the Federal Government who have a legitimate interest therein, and to United States citizens of known loyalty and discretion who of necessity must be informed thereof.

Classification Changed to
UNCLASSIFIED
Authority
DOD DIR 5200.10
Date 11/5/64 By L Dungca

NATIONAL ADVISORY COMMITTEE
FOR AERONAUTICS

WASHINGTON
August 25, 1950

CONFIDENTIAL

UNCLASSIFIED

SEP 5 1950

UNCLASSIFIED

NACA RM L50D04 CONFIDENTIAL

NATIONAL ADVISORY COMMITTEE FOR AERONAUTICS

RESEARCH MEMORANDUM

DETERMINATION BY THE FREE-FALL METHOD OF THE DRAG AND LONGITUDINAL STABILITY AND CONTROL CHARACTERISTICS OF A CANARD MODEL AT TRANSONIC SPEEDS

By Christopher C. Kraft, Jr. and Charles W. Mathews

SUMMARY

The stability and control characteristics and drag of a canard or tail-first configuration have been investigated by the free-fall method. This configuration was chosen in order to take advantage of a favorable interference effect on the drag of a swept wing-body combination by locating the wing behind the maximum body diameter. This favorable interference effect was indicated by a previous free-fall test.

In addition, an analysis of canard configurations indicates that such an arrangement may be expected to have satisfactory stability and control characteristics at transonic speeds. The test model had a sweptback wing and vertical tail, an all-movable horizontal control surface with a triangular plan form, and a fuselage of a high fineness ratio. An automatic control system was used to control the model longitudinally at a constant normal acceleration. The Mach number range covered by the test was from 0.7 to 1.27.

The drag characteristics of the canard configuration compared favorably with previous free-fall tests of a wing-body combination with the wing mounted rearward of the maximum body diameter. At a Mach number of 1.1 and a lift coefficient of 0.06 the drag coefficient of the model was 0.026. Because the lift coefficient was low for this flight condition, the value of drag coefficient obtained closely represents the minimum drag coefficient of the configuration. The favorable wing-body interference effects obtained by locating the wing rearward of the maximum body diameter were apparently unaltered by the incorporation of the horizontal control surface at the nose of the model.

The model had stick-fixed longitudinal stability throughout the test Mach number range, and no abrupt trim changes were encountered.

CONFIDENTIAL

UNCLASSIFIED

The model had a stable variation of pitching moment with angle of attack at all Mach numbers. The variation of pitching-moment coefficient with angle of attack became more negative with increasing Mach number up to a Mach number of 1.12. With further increase in Mach number this parameter became less negative and had the same value at a Mach number of 1.21 as at a Mach number of 0.8. In general, the stability and control characteristics of the model were good in the range of lift coefficients covered in the test (low lift coefficients).

The periods of the longitudinal oscillations of the model following the horizontal tail deflections were in good agreement with those calculated for this configuration using estimated stability derivatives. The damping of these oscillations was poor because of the high moment of inertia of the model, the low lift-curve slope of the horizontal control surface, and the small size of the model compared to a full-scale airplane.

INTRODUCTION

During the past several years a great deal of research has been directed toward the reduction of drag and the provision of satisfactory stability and control characteristics of airplanes designed to fly at transonic and supersonic speeds. Results of such investigations have indicated a number of possible modifications to the usual airplane configuration to improve the drag and/or the stability and control characteristics. In connection with one phase of this work, the reduction of interference drag between airplane components, free-fall tests have shown that some improvement in the drag of a swept wing-body combination can be obtained by locating the wing rearward of the maximum body diameter. (See reference 1.) Since this relative location of wing and body appears more suitable for use as a canard airplane (tail first) than as a conventional airplane (tail rearward), an analysis was made to investigate the stability and control characteristics of the canard arrangement. (See reference 2.) The results of this analysis indicate that the canard inherently possesses certain features which appear advantageous when considered from the standpoint of stability and control at transonic speeds. Accordingly, an investigation was undertaken to check experimentally the possibilities of the canard as a transonic airplane.

This paper presents results of a free-fall test of a canard configuration. The model tested incorporated an automatic pilot used to control the model longitudinally at a constant value of normal acceleration. An automatic lateral control system was also provided to maintain a constant but low value of rolling velocity during the test.

The data are presented herein as time histories of the measured quantities from which were obtained the lift and drag coefficients, lift-drag ratios, horizontal control-surface position required for trim during the test, and the variation of pitching moment with angle of attack as a function of Mach number. Tests have also been made by the NACA wing-flow method of this particular configuration (reference 3), and the tests reported herein give comparable data at higher Reynolds numbers.

APPARATUS AND METHOD

Model Configuration

The model tested was a canard or tail-first configuration as shown in figure 1. A three-view drawing showing the pertinent dimensions is presented in figure 2, and a complete list of dimensions is given in table I. The model had a 45° sweptback wing of aspect ratio 4.1, a triangular all-movable horizontal control surface of aspect ratio 2.0, a 45° sweptback vertical tail of aspect ratio 1.5, and a fuselage of fineness ratio 13.5.

The wing and vertical tail were made of solid duralumin. Both of these surfaces had a constant chord with an NACA 65-009 airfoil section perpendicular to the leading edge. (This section would have a thickness of 6.34 percent chord taken parallel to the air stream.) Details of the tip design of the wing and vertical tail, as well as details of the ailerons which were used for lateral control, are shown in figure 3. An airspeed head was mounted on a boom near the tip of the vertical tail, and a drawing of this installation is presented in figure 4.

Details of the horizontal control surface are also shown in figure 4. The horizontal control surface was made from a thin duralumin flat plate with an elliptical leading edge and a tapered trailing edge. The triangular horizontal control surface was chosen because theoretical and experimental investigations indicate a delta plan form to have low drag characteristics as well as satisfactory control effectiveness in the transonic and supersonic speed range. (See reference 4.)

The fuselage forward of the maximum diameter was geometrically similar to the bodies reported in reference 1 (fineness ratio of 12.0). The ordinates for this fineness-ratio-12 body were also used for the rearward section of the fuselage, but the length demensions were elongated to correspond to a fineness ratio of 15.0. The fuselage coordinates are given in table II. The fuselage at the fuselage-horizontal control-surface juncture was made flat-sided to minimize leakage through the juncture when the control surface was deflected from neutral. The gap between the horizontal control surface and fuselage was 0.01 inch.

The center of gravity of the model was located 81.7 percent of the mean aerodynamic chord (mean geometric chord) ahead of the leading edge of the mean aerodynamic chord. The model had a wing loading of 150 pounds per square foot and a moment of inertia about a lateral axis through the center of gravity of 531 slug-feet squared. The total horizontal control-surface deflection was from 0° to 12° trailing edge down. The total aileron deflection obtainable was 20° right and 8° left (right aileron 10° up, 4° down; left aileron 4° up, 10° down).

Control Systems

The automatic control systems and internal instrumentation used in this model are shown schematically in figure 5. An automatic pilot sensitive to normal acceleration was used to control the model in pitch. The automatic pilot operated in such a manner as to attempt to control the normal acceleration at approximately 1/2g. When the acceleration exceeded the desired 1/2g, the automatic pilot moved the horizontal control surface at a constant rate in the nose-down direction, and, in a like manner, when the acceleration fell below 1/2g, the automatic pilot moved the horizontal control surface in the nose-up direction. A $1\frac{1}{2}$-second time delay between control motion in one direction and the other was incorporated in the automatic pilot. This time delay eliminated any possibility of dynamic instability of the automatic pilot-model combination. This objective is accomplished by preventing any adverse phase relationship between motions of the horizontal control surface and the model.

In addition, a time delay of approximately 12 seconds was employed to prevent the automatic pilot from operating during the initial part of the drop. Use of the 12-second time delay allowed the model to increase in speed while at zero lift since the horizontal control surface was initially set at zero deflection. The increase in speed prior to control operation was desirable because the combination of a high wing loading and the low dynamic pressure at release might have resulted in a stall of the model.

Another automatic control system was used in attempt to control the rate of roll of the model. (See fig. 5.) The ailerons were connected by linkages to a rate gyro. The gyro restraining springs were preloaded to give a moment corresponding to the precessional moment produced by the gyro at a rate of roll of 1/10 rps. Since no roll existed at release, the ailerons were held by the spring preload at maximum deflection in the direction to produce right roll and remained so deflected until a rate of roll of approximately 1/10 rps was obtained, after which the gyro moved the ailerons in a direction to oppose further change in the rate of roll. The variation of precessional moment with rolling velocity for the gyro

used in this automatic control system was 52 inch-pounds per radian per second. The gyro had a moment of inertia of 0.07 inch-pound-second squared about the gimbal axis, and the gearing ratio between each aileron and the gyro was 0.35. The restraining springs at the gyro had a spring constant of 19 inch-pounds per radian about the gimbal axis and were preloaded to 33 inch-pounds.

One purpose of this lateral control system was to keep the rate of roll low so that the effect of roll on the longitudinal stability would be small or negligible. (See reference 5.) The other reason was to make sure that the model did roll so that its mean path would approximate a free fall. With the existence of a steady roll, the forces acting on the model rotate about the center of the helical path followed by the model during the drop and hence prevent the model from pulling out or appreciably deviating from the path normally followed by a body at zero lift.

Instrumentation and Measurements

The desired quantities were measured through use of the NACA radio-telemetering system and radar and phototheodolite equipment. The general arrangement of the internal instrumentation is shown in the schematic drawing of the model presented in figure 5. The following quantities were recorded at two separate ground stations by the telemetering system:

(1) Static and total pressure measured by an airspeed head connected to aneroid cells and mounted on a boom $1\frac{1}{2}$ chords ahead of the vertical tail at its tip (See figs. 1 and 4.)

(2) Normal and transverse accelerations and longitudinal retardation measured by three accelerometers alined with the respective axes of the model

(3) Horizontal control-surface position as measured by a control-position pickup

(4) Rate of roll as measured by motion pictures which were obtained during the entire fall of the model.

An attempt was also made to measure the rate of roll by a roll turn meter and the hinge moment of the horizontal control surface by a strain-gage pickup but these instruments failed to operate during the test.

The position of the model with respect to the ground axes was recorded during the entire drop by radar and phototheodolite equipment. A survey of atmospheric conditions applying to the test was obtained from

synchronized records of atmospheric pressure, temperature, and geometric altitude taken during the descent of the carrier airplane. The direction and velocity of the horizontal component of the wind was determined from radar and phototheodolite records obtained from the ascent of a free balloon immediately after the test.

Mach Number and Airspeed Measurements

The quantities which were used to determine the Mach number during the fall are presented as a time history in figure 6. The Mach number was obtained from the radar and phototheodolite data by first differentiating the flight path with respect to time to obtain the velocity of the model relative to the ground. The true airspeed was then found by a vector summation of this ground velocity and the measured horizontal wind velocity at coincident altitudes. This true airspeed was combined with the corresponding absolute temperature, as determined from the atmospheric survey, to obtain the Mach number.

The Mach number variation with time was also determined from the total pressure H measured by the airspeed head and the survey static pressure p. The following expression was used:

$$M = \sqrt{\frac{\left(\frac{H}{p}\right)^{\frac{\gamma-1}{\gamma}} - 1}{\frac{\gamma - 1}{2}}}$$

where the ratio of specific heat γ was taken as 1.4. The above expression does not account for the total pressure loss through the normal shock which occurs at supersonic speeds. However, this loss is negligible in the range of supersonic Mach numbers for which test results are presented. A comparison of the data obtained by the two independent methods is shown in figure 6. A discrepancy of approximately 0.03 Mach number is indicated between a Mach number of 0.85 to 1.15. This discrepancy increases to about 0.05 at the higher Mach numbers. In order to assure that this discrepancy was not due to lag in the line between the total pressure orifice and the pressure cell, calculations were made to determine this lag. The lag was found to be less than 0.01 second for any condition of the test and this amount of lag would have a negligible effect on the measured Mach number. A similar discrepancy has been obtained in previous free-fall tests, especially at the higher

Mach numbers (see reference 1), but as yet the cause for this difference is unexplained. All results presented in this paper are based on the radar Mach number shown in figure 6 which is believed accurate to within ±0.01 Mach number.

The static-pressure error of the airspeed head $\Delta p/q$ as a function of Mach number is shown in figure 7. The error presented is the difference between telemeter and survey static pressure expressed as a fraction of dynamic pressure. The telemeter static pressure was that measured by the airspeed head mounted in front of the vertical tail. Although the variation shown in figure 7 is not a true calibration of the airspeed head because of possible errors in telemeter transmission, the data are indicative of the type of static-pressure error that would be expected from an airspeed installation located in this region. This variation in static-pressure error is caused chiefly by the pressure field of the body. The results of data obtained in reference 6 indicate that the pressure coefficient on a similar body at about 80-percent body length, which is the approximate location of the airspeed head on this model, increases in a positive direction up to a Mach number of about 1.0, and then at a Mach number of approximately 1.0, a shock wave passes this particular body station resulting in a sudden drop in pressure coefficient. Thereafter, the pressure is negative. The magnitudes of the pressure variations obtained in this test are of the same order as those presented in reference 6. The passage of the shock wave over the static orifices of the airspeed boom of this model seems to occur at about 0.03 Mach number before that shown in reference 6 for a similar body station. The pressure field produced by the wing of the canard model might account for this difference.

Reduction of Data

The various coefficients presented in this paper were determined from the values of model weight W, wing area S, normal acceleration n (in g units), static pressure p, and Mach number M. The following relationship was applied to obtain the normal-force coefficient C_N:

$$C_N = \frac{Wn}{Sp\frac{\gamma}{2}M^2}$$

The chord-force coefficient C_C was calculated from the same relation using the longitudinal retardation.

The lift coefficient C_L and drag coefficient C_D were calculated by resolving the normal-force and chord-force coefficients perpendicular and parallel to the wind axis. The angles of attack involved in the computations of C_L and C_D were determined from the lift-curve slopes obtained from wing-flow tests of the same configuration (reference 3). The variation of pitching-moment coefficient with angle of attack $dC_m/d\alpha$ was calculated by use of the equation

$$\frac{dC_m}{d\alpha} = \frac{(2\pi f)^2 I}{\frac{\gamma}{2} M^2 p S \bar{c}}$$

where f is the frequency of the oscillation of the model in pitch, I is the moment of inertia of the model about a lateral axis through the center of gravity, and $\bar{c}$ is the mean aerodynamic chord. The effects of aerodynamic damping and the additional degree of freedom (motion along the Z-axis) on the frequency were neglected because these effects were found negligible for this model.

RESULTS AND DISCUSSION

Basic Results

A time history of the quantities measured during this test is shown in figure 8. The horizontal control-surface position, normal and transverse accelerations, and longitudinal retardation were determined from the telemeter records. The rate of roll was evaluated from the variation of the roll attitude of the model with time as determined from motion pictures taken during the fall. The variation of Mach number and Reynolds number with time is also presented in figure 8. The Reynolds number of the test varied from approximately 2,000,000 at release to about 16,000,000 at impact.

The horizontal control-surface position during the first 12 seconds of the drop remained at approximately 0° because of the time delay previously described. The normal acceleration during this period gradually increased to about 0.2g. This deviation from the desired zero-lift fall was probably due to a slight rigging misalinement of the model, since the model was symmetrical in design with the exception of the vertical tail. The pitching moment due to drag of the vertical tail was investigated as a possible cause for this gradual increase in normal acceleration, but the computations indicate that no significant change in the trim value of normal acceleration could have resulted from this effect.

After the time delay, the horizontal control surface went to a large nose-up deflection (trailing edge down). Since the rate of control movement produced on a signal from the automatic pilot was high compared to the corresponding response of the model in pitch, the control had a tendency to overshoot the required trim position, and, as shown by figure 8, this initial control-surface deflection was greater than the deflection required to trim at the desired 1/2g as the normal acceleration reached approximately 1g. Following the initial control movement, the horizontal control-surface deflection was rapidly reduced and the normal acceleration thereafter remained near 1/2g through a main part of the fall. The control deflection required to maintain this value of normal acceleration showed a progressive tendency to decrease as the Mach number increased. This progressive movement of the horizontal control surface toward zero deflection proved the model to be longitudinally stable stick-fixed for the range of speeds tested.

Above a Mach number of 1.20, no additional nose-down control-surface deflection was available. Supposedly, the horizontal control surface should have returned to zero deflection at the same time the automatic pilot reached its down stop. However, a small amount of nose-up deflection still existed under these conditions which was probably due to a slight shift in the automatic control stops. Had lower control-surface deflections been available, the model could have been controlled at 1/2g up to impact, but because the control surface apparently could not return to zero the normal acceleration gradually increased from about 1/2g at 38.5 seconds from release to 2.3g at impact.

The oscillations in pitch following horizontal control-surface deflections during the controlled period of the drop were poorly damped and this phenomenon is discussed subsequently. The time history of the normal acceleration and other measured quantities shown in figure 8 are of necessity reduced in scale from the actual variations obtained on the telemeter records, and the smooth wave form of the pitching oscillations was lost to some extent in the transcribing process. A portion of the telemeter record showing a typical oscillation in pitch following a horizontal control-surface deflection is shown in figure 9. The actual telemeter record was used in reduction of the measured data which allowed a much higher degree of accuracy than is indicated by the time history of figure 8.

The longitudinal retardation remained near zero during the time-delay period following release. Then, as the model pitched to a positive angle of attack, the longitudinal retardation increased to a small positive value due to the associated induced drag of the wing and horizontal control surface. The retardation remained low up to a Mach number of approximately 0.9. At this Mach number, the retardation began a gradual rise which continued until ground impact.

The transverse acceleration shown in figure 8 indicates the model was in a right sideslip during the first 7 seconds of the fall. The transverse acceleration during the remainder of the drop was near zero. The time history of transverse acceleration indicates that the lateral motion of the model was well damped throughout the Mach number range tested. The abrupt steps in the transverse acceleration record shown in figure 9 were used to indicate the operating sequence of the longitudinal automatic control system. The automatic control signal was superimposed on the transverse acceleration channel in such a manner as to cause the trace to step a constant increment whenever the automatic control signal reversed direction.

The model began to roll immediately after release from the carrier airplane and attained a rolling velocity of about 4 radians per second. This high rate of roll continued up to approximately 14 seconds after release and then rapidly decreased to about 0.4 to 0.6 radian per second. The lateral control provided by the automatic control system was set to control the model at approximately 0.6 radian per second. It is obvious that the automatic control did not operate during the first 14 seconds of the drop, but thereafter began to control the rate of roll of the model. The reason for loss of control during the initial period is not definitely known, but possibly the aileron control linkages were jammed which prevented the automatic control from operating. The ability of the ailerons to control the rate of roll after 14 seconds from release indicates that the ailerons remained effective throughout the range of Mach numbers tested.

Experimental Coefficients

The variations of normal-force coefficient, lift coefficient, chord-force coefficient, drag coefficient, and lift-drag ratio as a function of Mach number are presented in figure 10. Since after each horizontal control-surface deflection there was an oscillation in pitch, the forces acting on the model also oscillated. The values of the coefficients shown in figure 10 are a faired average of the maximum and minimum values obtained during an oscillation. The drag coefficient was not presented below a Mach number of 0.8 because of the possible inaccuracy involved in estimating the angle of attack at high lift coefficients. The normal-force and lift coefficients varied from about 0.62 at a Mach number of 0.73 to 0.05 at a Mach number of 1.15, generally decreasing as the Mach number increased. Above a Mach number of 1.15 these coefficients gradually increased to about 0.1 at a Mach number of 1.25.

Near a Mach number of 0.85 the drag coefficient rose abruptly from 0.02 to about 0.03. An approximate calculation of the drag at this Mach number and lift coefficient indicates that this abrupt drag rise was due chiefly to the induced drag of the horizontal control

surface. This large amount of induced drag was a result of the high control-surface deflections required for trim because of the high degree of static stability used in this test. When the lift coefficient again decreased (between Mach numbers of 0.90 and 0.95) the drag coefficient also decreased to about 0.021. The drag coefficient then rose abruptly to about 0.026 at a Mach number of 1.0, remained effectively constant between Mach numbers of 1.0 and 1.15, and then gradually increased as the lift coefficient increased at higher Mach numbers.

The highest lift-drag ratio obtained in the test was about 8.8 which occurred between Mach numbers of 0.85 to 0.95 and at lift coefficients of 0.27 to 0.18. The lift-drag ratios shown in the figure do not represent the maximum lift-drag ratio L/D that could be obtained with this model, especially at the higher Mach numbers, because the test lift coefficients were low. In order to obtain some indication of the maximum lift-drag ratios that might be expected with this configuration, an approximate calculation of the maximum lift-drag ratios was made. The results of these calculations are presented in the appendix.

Zero-Lift Drag Calculations

The zero-lift drag coefficients of the test configuration have been estimated using the test data as a basis for the computations. In order to determine the zero-lift drag, the part of the measured drag attributable to lift was estimated. The following method was used in making this estimation. At subsonic Mach numbers the angle of attack of the model corresponding to each test lift coefficient was estimated from results of the wing-flow tests of the same configuration (reference 3). Then, knowing the control-surface deflections, the lift coefficient of the horizontal control surface as well as the wing were estimated. Using these lift coefficients the induced drag of the wing and horizontal control surface were determined separately and added to obtain the total induced drag. The drag of the horizontal control surface was estimated from the data presented in reference 7. These data are for a 60° triangular wing with a section approximately the same as that used on the canard model. Although the data presented in reference 7 were obtained at low subsonic Mach numbers, these data were assumed to indicate satisfactorily the variation of drag with lift of the horizontal control surface over the higher range of subsonic Mach numbers applying to the present test. The usual formula $C_{L_W}{}^2/\pi A$, where C_{L_W} is the lift coefficient of the wing and A is the aspect ratio, was assumed to calculate the induced drag of the wing. The effect of the wing and control surface were considered separately because of the large control-surface deflections which existed at subsonic Mach numbers. The method used, however, does not account for interference effects between the components of the model.

The drag due to lift at supersonic Mach numbers was calculated by the method presented in reference 8. In this method, the total airplane lift coefficient was employed which assumed that the variation of drag coefficient with lift coefficient for the complete model was the same as the theoretical variation presented in reference 8 for a wing alone. Although this method would probably underestimate the drag due to lift of the canard model for the conditions where the control surface is operating at large deflections, it is felt that the zero-lift drag coefficients of the canard model have been determined with good accuracy at Mach numbers above 1.0 because during the test the tail deflections were small and the lift coefficients were low in this Mach number range. It should also be pointed out that the data presented in reference 8 for drag due to lift are for a uniformly loaded wing with a correction for loss in lift at the tips. Since the lift coefficients of the canard model at supersonic speeds were low, however, the application of this data to an untwisted wing of the type incorporated in the canard model is believed to be of sufficient accuracy for purposes of determining the zero lift-drag coefficients. The drag due to lift at a Mach number of 0.90 amounted to approximately 40 percent of the total measured drag and at a Mach number of 1.10 amounted to approximately 2.5 percent of the total measured drag. The zero-lift drag coefficients determined by this method are presented as a function of Mach number in figure 11.

A comparison between the zero-lift drag coefficients based on the test results and those predicted by supersonic theory is shown in figure 12. The pressure drag coefficient for each component of the canard configuration has been computed along with the total-skin-friction drag. A summation curve of the total predicted drag coefficient is also presented. The pressure drag of the wing and vertical tail was computed from reference 9, the pressure drag of the fuselage was computed from reference 10, and the drag due to skin friction was computed from references 11 and 12. (These methods neglect compressibility effects.) In making the calculations of the pressure drag of the vertical tail, the fuselage was assumed to act as a reflection plane and the drag coefficient was computed as though the vertical tail was symmetrical with respect to the body center line. The drag computations for the wing were based on the exposed wing geometry. The fuselage again was assumed to act as a reflection plane. The pressure drag of the horizontal control surface was calculated by use of reference 13 but was found to be negligible for the Mach number range tested. The agreement between the experimental and theoretical drag appears good at Mach numbers above the drag rise up to a Mach number of 1.10. The theory overestimates the drag for all test Mach numbers above 1.10. Although the theory appears able to predict the drag coefficient accurately up to a Mach number of 1.10, it should be noted that the theory does not account for the interference effects between the airplane components. These interference effects have been shown in reference 1 to be very important, especially at Mach numbers above 1.0. The discrepancy above a Mach number of 1.10 between

the experimental and theoretical drag coefficient is a result of the increase in pressure drag of the wing and vertical tail predicted by the theory as the Mach lines approach the leading edge of the wing and tail. This increase in drag coefficient either did not occur or was of a much smaller magnitude than that predicted by theory. Similar comparisons between experiment and theory have been made for other free-fall models and similar discrepancies are indicated. (See reference 14.) It should be noted that the airfoil section of the canard wing and the wings of reference 14 have a rounded leading edge, whereas the calculations of reference 9 apply strictly to circular-arc sections (sharp leading edge).

The zero-lift drag coefficient of the canard model and several other configurations is presented for comparison in figure 13. The configurations presented for comparison are the Bell X-1 drop model reported in reference 15, a rocket model of a transonic airplane configuration, and two wing-body combinations reported in reference 1. Since the Bell X-1 model and the rocket model were also tested under lifting conditions, the drag due to lift was estimated and then subtracted from the measured drag in order to determine the zero-lift drag coefficient. The drag due to lift at subsonic Mach numbers was estimated by the usual formula $C_L^2/\pi A$. At supersonic Mach numbers the same procedure used to calculate the drag due to lift of the canard model was employed.

The zero-lift drag coefficients of the canard model were much lower than the drag coefficients for the Bell X-1 drop model and the transonic rocket model. The comparison between the canard model and the two wing-body combinations shows that the drag coefficients were of the same order of magnitude. The two wing-body combinations differed only in the location of the wing on the body, one having the wing mounted forward of the maximum body diameter and one having the wing mounted to the rear of the maximum body diameter. The difference in the drag coefficients of these two wing-body combinations, which is evident in figure 13, was shown in reference 1 to result primarily from a favorable interference effect of the wing on the body drag when the wing was mounted in this rearward position. The canard model was designed in hopes of realizing this favorable interference effect.

The canard model would be expected to have a higher drag coefficient (based on wing area) than the wing-body combination with the wing mounted rearward of the maximum body diameter because of the increased ratio of surface area to wing plan area and the additional pressure drag of the vertical and horizontal tail surfaces. Calculations of the drag coefficient of these various components at a Mach number of 1.20 indicated that the following increases in drag coefficient would be expected: a 13-percent increase in the total drag coefficient because of a one-fourth greater ratio of surface area to wing plan area and an increase of approximately 8 percent in the total drag coefficient as a result of

the pressure drag of the vertical tail. The increase in total drag coefficient as a result of the pressure drag of the horizontal control surface was found to be negligible. There are also several factors which decrease the drag coefficient of the canard model relative to the wing-body combination. The increased fineness ratio of the canard fuselage caused a slight reduction in pressure drag coefficient which amounted to approximately 2 percent of the total drag coefficient. (See reference 16.) An increase in Reynolds number for a given Mach number because of the increased scale of the canard model and a lower release altitude resulted in a 4-percent decrease in the total drag coefficient. The summation of these effects indicates that at a Mach number of 1.20 the total drag coefficient for the canard model would be 15 percent higher than that for the wing-body combination. The increase shown by the comparison of the test results at a Mach number of 1.20 is 17 percent. This agreement between the measured and predicted increase in drag coefficient indicates that the interference effects obtained for the wing-body combination were also obtained for the canard model and that this favorable interference effect was apparently unaltered by the presence of the horizontal control surface at the nose of the canard fuselage.

Longitudinal Stability and Trim Characteristics

The variation of horizontal control-surface angle required for trim with Mach number is shown in figure 14. A similar plot is shown of the horizontal control-surface angle required for trim as obtained by the wing-flow tests of this configuration. (See reference 3.) The trim lift coefficients of the free-fall tests were used to compute the horizontal control-surface deflections required for trim from the wing-flow data. These lift coefficients are also presented in figure 14. The increasing down control-surface deflection required for trim with increasing Mach number shows the airplane to be longitudinally stable stick fixed over the test Mach number range. The smooth variation in horizontal control-surface incidence required for trim also indicates that no abrupt trim changes were experienced. The same variation in horizontal control-surface incidence required for trim is shown by the data calculated from the wing-flow tests indicating good agreement between the two test methods. It should be pointed out that the data for the free-fall model were obtained under conditions where the altitude was changing rapidly and therefore does not correspond to the usual static-stability test where the altitude is maintained approximately constant. Similar but smaller variations in horizontal control-surface incidence required for trim would be obtained in a level-flight condition.

The periods of the longitudinal oscillations performed by the model following a deflection of the horizontal control surface are presented in figure 15. An accurate determination of the damping of these

oscillations could not be obtained from the telemeter records because of the poor damping of the model and relatively short time following each horizontal control-surface deflection. (See fig. 9.) Calculations were made prior to the test of the period and damping of the natural short-period longitudinal oscillations for this model configuration using estimated stability derivatives, and the computed values are also shown in the figure. Good agreement is indicated between these calculated values and the test results for the period of the oscillations. It should be noted that a constant value of pitching-moment variation with angle of attack was used in making the calculations prior to the test.

The test model had a large value of pitching-moment variation with angle of attack compared to the values usually used in most conventional airplane designs. This large amount of static stability would normally result in shorter periods than those shown, provided a normal wing loading had been used, but because the wing loading of the test model was very high, (150 lb/sq ft) the inertia of the model was large and counteracted the effect of the high $dC_m/d\alpha$ on the period. The poor damping of these oscillations was caused by the high moment of inertia, the relatively low lift-curve slope of the triangular horizontal control surface, and the small size of the model compared to a full-scale airplane. Similar results were obtained in tests of the Bell X-1 drop model (see reference 15) although the damping was slightly higher because of the higher lift-curve slope of the horizontal control surface.

The calculated damping for the test configuration is presented in figure 15 as the time to damp to one-half amplitude and the cycles to damp to one-tenth amplitude. The flying-qualities requirements of reference 17 require the airplane to damp to one-tenth amplitude in one cycle. It is obvious that the model tested would not meet this requirement. In order to estimate the period-damping relationship for a configuration such as the one tested with a normal wing loading and scale comparable to a fighter airplane, similar calculations were made for a wing loading of 50 pounds per square foot and the scale of the model increased by a factor of 5. The period-damping relationship of the configuration with these modifications was very much improved, but not sufficiently to meet the requirements of reference 17. The damping could be improved further by using a horizontal control surface with a higher aspect ratio and hence a higher lift-curve slope. This modification would result in a larger damping contribution from this component.

The variation of the static-longitudinal-stability parameter $dC_m/d\alpha$ with Mach number is presented in figure 16. The model was statically stable for the entire Mach number range shown. The stability increased with increasing Mach number between Mach numbers of 0.8 to 1.12. From a Mach number of 1.12 to 1.21 the stability decreased to approximately the same value as was obtained at a Mach number of 0.8. The value of $dC_m/d\alpha$ obtained at a Mach number of 0.74 was for a different lift-coefficient

range than the other test points shown in figure 16 and should not be misconstrued as a wild point. (Note the high lift coefficient at this Mach number.)

In order to determine whether the decrease in static stability in the high Mach number range resulted from flexibility of the sweptback wing, the test data were transformed to the case for a rigid wing by an approximate method. The angle-of-attack changes along the wing span due to the wing bending under load were computed by assuming that the aerodynamic load was uniformly distributed along the wing span. The change in loading corresponding to these angle-of-attack changes was determined as a function of lift coefficient and dynamic pressure by use of strip theory. The change in lift-curve slope of the wing as well as the shift in aerodynamic center of the wing were predicted from these loading changes, and the test data were then corrected to eliminate these effects on the stability of the model. The effect of torsional deflections of the wing was not included in the analyses because the effects of wing bending were found to greatly predominate. The effects of control-surface flexibility were not considered since the control surface was relatively stiff compared to the wing. The fuselage was extremely rigid and no aero-elastic effects are believed to have been produced from this source. The variation of $dC_m/d\alpha$ with Mach number for this rigid-wing condition is also shown in figure 16. Transforming the data to the case of a rigid wing results in an increase in stability at all Mach numbers. Although the increase becomes greater at the higher Mach numbers, the same type of stability variation with Mach number is obtained for the rigid-wing condition as from the test data. Therefore, the wing deformation at the high Mach numbers does not appear to account entirely for the decrease in stability associated with this model.

The decrease in stability at the high Mach numbers is probably due chiefly to the increased horizontal control-surface effectiveness which was indicated by the wing-flow tests and possibly a decrease in the lift-curve slope of the wing as the Mach lines approach the leading edge of the wing. A rearward movement of the aerodynamic center usually occurs on sweptback wings at transonic speeds and would result in increased stability for this configuration. However, the decrease in stability brought about by the possible decrease in lift-curve slope of the wing and the increased control-surface effectiveness is apparently larger than the increase in stability caused by this aerodynamic-center shift.

CONCLUDING REMARKS

The stability and control characteristics and drag of a canard configuration have been investigated by the free-fall method. The model had a 45° sweptback wing and vertical tail, a triangular

all-movable horizontal control surface and a fuselage of fineness ratio 13.5. The model was controlled longitudinally at approximately 1/2g normal acceleration by an automatic pilot. The Mach number range covered by the test was from 0.7 to 1.27.

The transonic drag characteristics of this model at zero lift were as favorable as any other configuration previously tested by the free-fall method. The zero-lift drag coefficient of this model was much lower than those obtained from previous tests of several models of present-day transonic airplane configurations employing either straight or swept wings. The drag coefficient of the model at a Mach number of 1.1 and a lift coefficient of 0.06 was 0.026. This value of drag coefficient closely represents the minimum drag coefficient for this Mach number because the lift coefficient was low for this flight condition. The favorable wing-body interference effects obtained in a previous test of a wing-body combination by locating the wing rearward of the maximum body diameter did not appear altered in the case of the canard model by the presence of the horizontal control surface at the nose of the model.

In general, the longitudinal stability and control characteristics of the model were very satisfactory for the range of Mach numbers and lift coefficients covered by the test. The results of the test indicate that the model was stable stick fixed for the Mach number range tested and that no abrupt trim changes were experienced. The periods of the longitudinal oscillations performed by the model following horizontal control-surface deflection were in good agreement with those calculated prior to the test. The oscillations were poorly damped as a result of the high moment of inertia of the model, the low lift-curve slope of the horizontal control surface, and the small size of the model compared to a full-scale airplane.

The model had a stable variation of pitching moment with angle of attack throughout the Mach number range. The stability increased between Mach numbers of 0.8 to 1.12, and from Mach numbers of 1.12 to 1.21 decreased to approximately the same value obtained at a Mach number of 0.8. The decrease in stability at the higher Mach numbers was believed to be caused by the increased horizontal control-surface effectiveness and the possible decrease in lift-curve slope of the wing as the Mach lines approached the leading edge of the wing. An approximate calculation of the effect of wing deformation showed that the stability was decreased

by this effect, especially at the higher Mach numbers, but that the general variation of static stability with Mach number was not affected.

Langley Aeronautical Laboratory
National Advisory Committee for Aeronautics
Langley Air Force Base, Va.

APPENDIX

ESTIMATED LIFT-DRAG RATIOS

The zero-lift drag coefficients presented in figure 11 form a basis for computation of lift-drag polars which more completely defines the drag characteristics of the test model. Estimates of the variation of drag with lift corresponding to a condition of small control-surface incidence have been made at supersonic speeds by the method presented in reference 8, while at subsonic speeds corresponding data were obtained from wind-tunnel tests of a wing-body combination having sweepback, aspect ratio, and thickness ratio comparable to the canard model. (See reference 18.) The variations of drag with lift so determined were faired through the zero-lift drag points to determine the estimated lift-drag polars for the test model. These polars are presented in figure 17 for several Mach numbers. It should be noted that an efficiency factor of 1.0 was used in making these calculations.

The theory outlined in reference 8 for obtaining the effect of lift on drag at supersonic speeds applies to a wing alone. In the calculations discussed in the preceding paragraph this theory was assumed to apply for the complete model in the determination of the lift-drag polars. It is believed, however, that the presence of a fuselage and a horizontal control surface would result in only minor modifications to the lift-drag polars and a slight reduction in maximum lift-drag ratio provided the control surface is at small incidence. Conditions of high stability where the variation of control-surface deflection with trim lift coefficient is large would invalidate the use of this method because the horizontal control surface would operate at large lift coefficients and its contribution to the total drag due to lift would be large compared to the wing. Another point worth noting is that although tests have shown the theory of reference 8 to predict satisfactorily the drag due to lift for untwisted wings with no appreciable flow separation, it cannot be expected to apply where separation occurs. The wind-tunnel-test results used in determining the lift-drag polars of the test model at subsonic speeds (reference 18) show no evidence of appreciable separation up to lift coefficients close to the maximum lift coefficient. Because the Reynolds numbers of the canard test were appreciably higher than those of the wind-tunnel tests, it was assumed that no separation would occur on the wing of the canard model.

The maximum lift-drag ratios predicted from the polars presented in figure 17 are presented in figure 18. The maximum lift-drag ratio obtained in this manner is 13.4 at a Mach number of 0.95 and a lift coefficient of 0.40. The maximum lift-drag ratio decreases to 10.5 at

a Mach number of 1.05 and a lift coefficient of 0.5 and further decreases with increasing Mach number to a value of 8.0 at a Mach number of 1.25 and a lift coefficient of 0.45.

REFERENCES

1. Mathews, Charles W., and Thompson, Jim Rogers: Comparison of the Transonic Drag Characteristics of Two Wing-Body Combinations Differing Only in the Location of the 45° Sweptback Wing. NACA RM L7I01, 1947.

2. Mathews, Charles W.: Study of the Canard Configuration with Particular Reference to Transonic Flight Characteristics and Low-Speed Characteristics at High Lift. NACA RM L8G14, 1949.

3. Crane, Harold L., and Adams, James J.: Wing-Flow Measurements of Longitudinal Stability and Control Characteristics of a Canard Airplane Configuration with a 45° Sweptback Wing and a Triangular All-Movable Control Surface. NACA RM L50A31, 1950.

4. Jones, Robert T.: Properties of Low-Aspect-Ratio Pointed Wings at Speeds below and above the Speed of Sound. NACA Rep. 835, 1946.

5. Phillips, William H.: Effect of Steady Rolling on Longitudinal and Directional Stability. NACA TN 1627, 1948.

6. Thompson, Jim Rogers: Measurements of the Drag and Pressure Distribution on a Body of Revolution throughout Transition from Subsonic to Supersonic Speeds. NACA RM L9J27, 1950.

7. Riebe, John M., and Fikes, Joseph E.: Preliminary Aerodynamic Investigation of the Effect of Camber on a 60° Delta Wing with Round and Beveled Leading Edges. NACA RM L9F10, 1949.

8. Jones, Robert T.: Estimated Lift-Drag Ratios at Supersonic Speed. NACA TN 1350, 1947.

9. Harmon, Sidney M., and Swanson, Margaret D.: Calculations of the Supersonic Wave Drag of Nonlifting Wings with Arbitrary Sweepback and Aspect Ratio. Wings Swept behind the Mach Lines. NACA TN 1319, 1947.

10. Thompson, Jim Rogers: A Rapid Graphical Method for Computing the Pressure Distribution at Supersonic Speeds on a Slender Arbitrary Body of Revolution. NACA TN 1768, 1949.

11. Squire, H. B., and Young, A. D.: The Calculation of the Profile Drag of Aerofoils. R. & M. No. 1838, British A.R.C., 1938.

12. Young, A. D.: The Calculation of the Total and Skin Friction Drags of Bodies of Revolution at Zero Incidence. R. & M. No. 1874, British A.R.C., 1939.

13. Puckett, A. E., and Stewart, H. J.: Aerodynamic Performance of Delta Wings at Supersonic Speeds. Jour. Aero. Sci. vol. 14, no. 10, Oct. 1947, pp. 567-578.

14. Thompson, Jim Rogers, and Mathews, Charles W.: Effect of Wing Sweep, Taper, and Thickness Ratio on the Transonic Drag Characteristics of Wing-Body Combinations. NACA RM L8K01, 1948.

15. Matthews, James T. Jr., and Mathews, Charles W.: Determination by the Free-Fall Method of the Longitudinal Stability and Control Characteristics of a $\frac{1}{4}$-Scale Model of the Bell XS-1 Airplane at Transonic Speeds. NACA RM L8G29a, 1948.

16. Thompson, Jim Rogers, and Kurbjun, Max C.: Drag Measurements at Transonic Speeds of Two Bodies of Fineness Ratio 9 with Different Locations of Maximum Body Diameter. NACA RM L8A28b, 1948.

17. Anon.: Specification for Flying Qualities of Piloted Airplanes. NAVAER SR-119B, Bur. Aero., June 1, 1948.

18. Salmi, Reino J., Conner, D. William, and Graham, Robert R.: Effects of a Fuselage on the Aerodynamic Characteristics of a 42° Sweptback Wing at Reynolds Numbers to 8,000,000. NACA RM L7E13, 1947.

TABLE I.- DIMENSIONS OF CANARD DROP MODEL

Wing:	
Area (includes area covered by fuselage), sq ft	11.88
Span, ft	7.0
Aspect ratio	4.1
Sweepback, deg	45
Chord (normal to leading edge), ft	1.2
Mean aerodynamic chord, ft	1.695
Mean aerodynamic chord location (leading edge at fuselage station)	94.825
Airfoil section (normal to leading edge)	NACA 65-009
Taper ratio	1.0
Aileron area (one aileron rearward of hinge line), sq ft	0.288
Aileron horn balance area (ahead of hinge line), sq ft	0.056
Aileron span (perpendicular to fuselage center line), ft	1.138
Aileron chord (normal to leading edge), ft	0.1795
Aileron deflection (total), deg	20° right and 8° left (i.e., right aileron 10° up and 4° down; left aileron 10° down and 4° up)
Horizontal control surface:	
Area (includes area covered by fuselage), sq ft	2.0
Span, ft	2.0
Aspect ratio	2.0
Root chord, ft	2.0
Mean aerodynamic chord, ft	1.333
Airfoil section - $\frac{1}{2}$-in. flat plate with round leading edge (normal to leading edge) and tapered trailing edge	
Hinge line (forward of trailing edge), ft	0.736
Deflection (trailing edge down), deg	0 to 12
Vertical tail:	
Area (includes area covered by fuselage above fuselage center line), sq ft	2.125
Span, ft	1.785
Aspect ratio	1.5
Sweepback, deg	45
Chord (normal to leading edge), ft	0.842
Mean aerodynamic chord, ft	1.19
Airfoil section (normal to leading edge)	NACA 65-009
Taper ratio	1.0

TABLE I.- DIMENSIONS OF CANARD DROP MODEL - Concluded.

Fuselage:	
Length (basic), ft	13.5
Side area, sq ft	9.24
Surface area, sq ft	29.20
Maximum diameter, ft	1.0
Location of maximum diameter	Fuselage station 72
Other general specifications:	
Center-of-gravity position	Fuselage station 78.19
Weight, lb	1770
Moment of inertia about lateral axis, slug-ft^2	531
Wing location - intersection of 50-percent-chord line with body center line at fuselage station	84.0
Horizontal control-surface location - hinge line at fuselage station	7.5
Vertical tail location - intersection of 50-percent-chord line with body center line at fuselage station	132.3

TABLE II.- FUSELAGE COORDINATES

Side view		Plan view	
Fuselage station	Radius	Fuselage station	Y
0.000	0.000	0.000	0.000
.72	.332	.720	.332
1.08	.430	1.08	.430
1.80	.617	1.80	.617
3.60	1.039	3.60	1.039
7.20	1.735	7.20	1.735
10.80	2.323	[a]7.50	1.790
14.4	2.836	[a]17.0	2.48
21.6	3.734	22.0	3.30
28.8	4.450	25.0	3.726
36.0	4.990	28.0	4.081
43.2	5.387	31.0	4.391
50.4	5.663	34.0	4.671
57.6	5.851	37.0	4.931
64.8	5.965	40.0	5.156
72.0	6.000	43.0	5.356
81.0	5.946	45.0	5.451
90.0	5.794	50.4	5.663
99.0	5.532	57.6	5.851
107.5	5.129	64.8	5.965
117.0	4.505	72.0	6.000
126.0	3.637	81.0	5.946
135.0	2.666	90.0	5.794
143.0	1.620	99.0	5.532
153.0	.631	107.5	5.129
162.0	.000	117.0	4.505
		126.0	3.637
		135.0	2.666
		143.0	1.620
		153.0	.631
		162.0	.000

[a] Fuselage is straight line between these two stations.

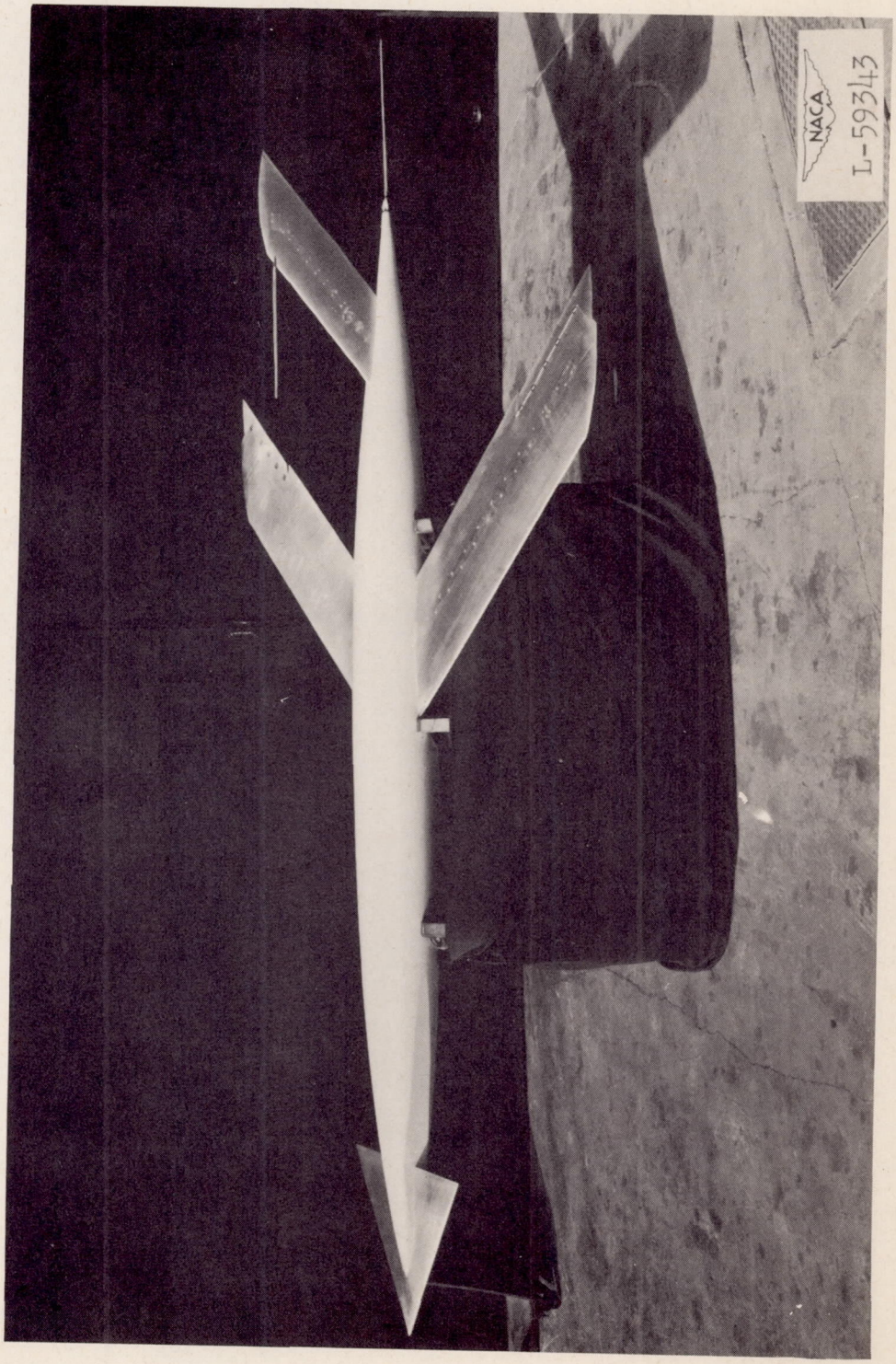


Figure 1.- Side view of the canard model.

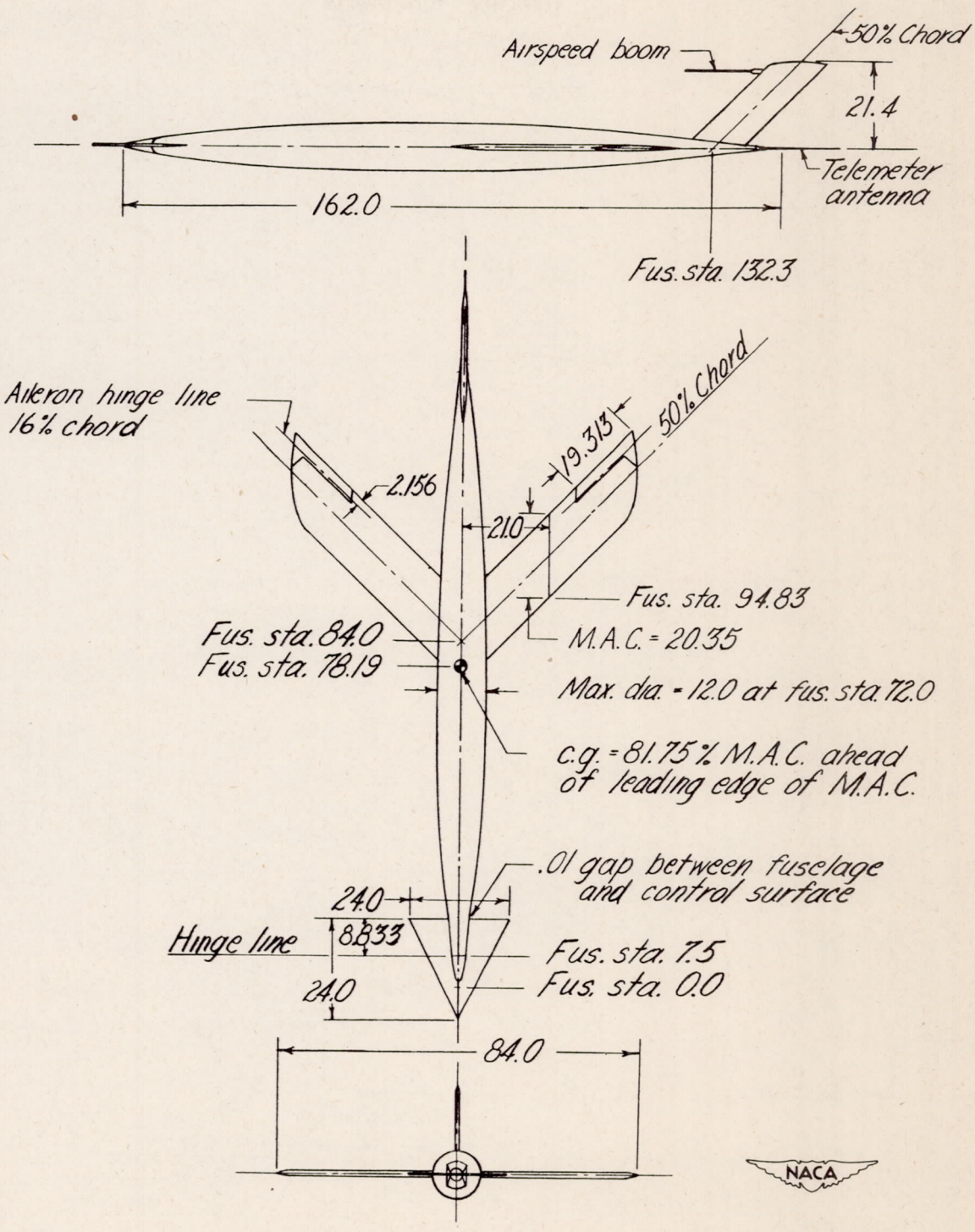


Figure 2.– Three–view drawing of the canard model. All dimensions are in inches.

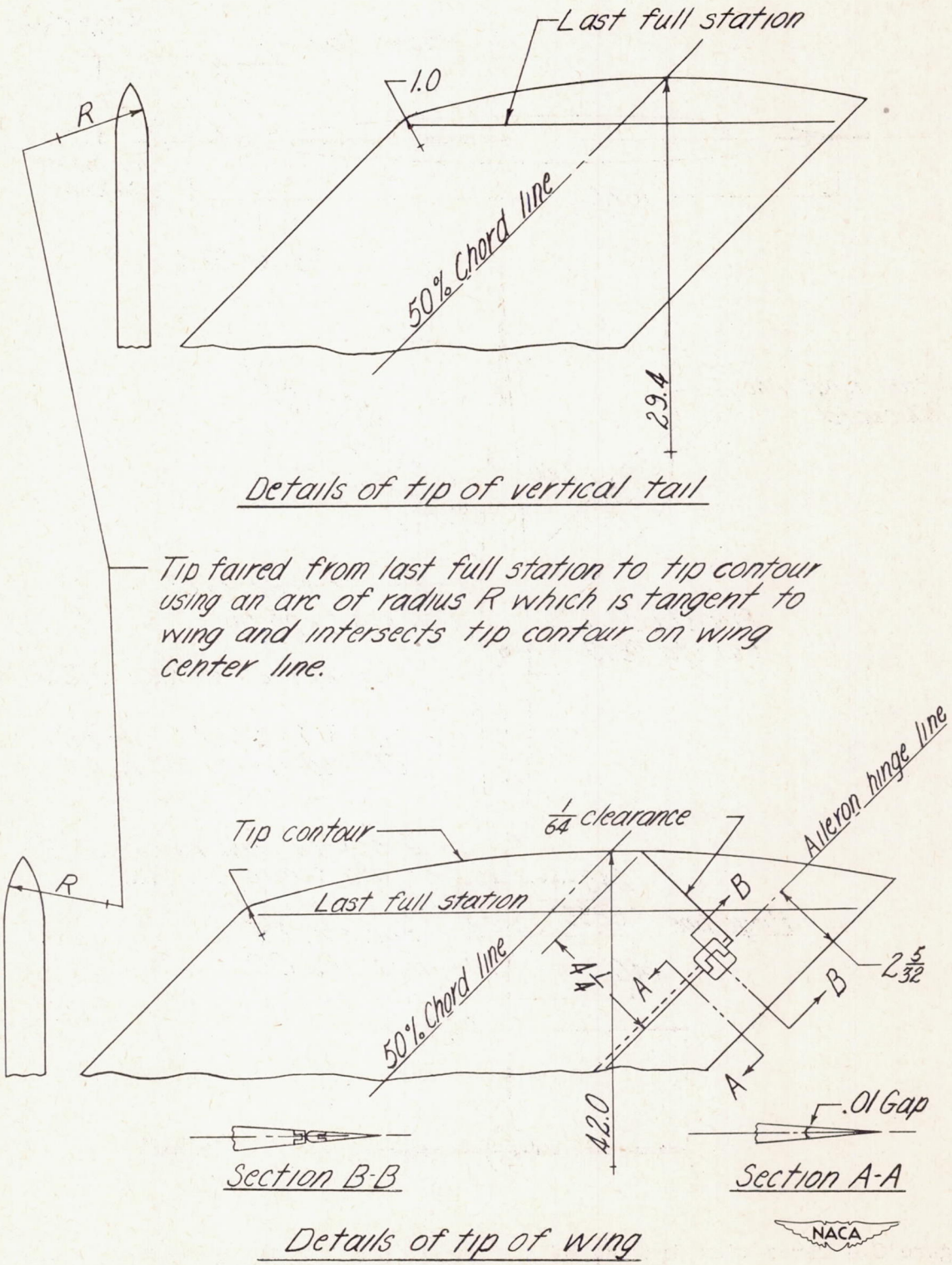
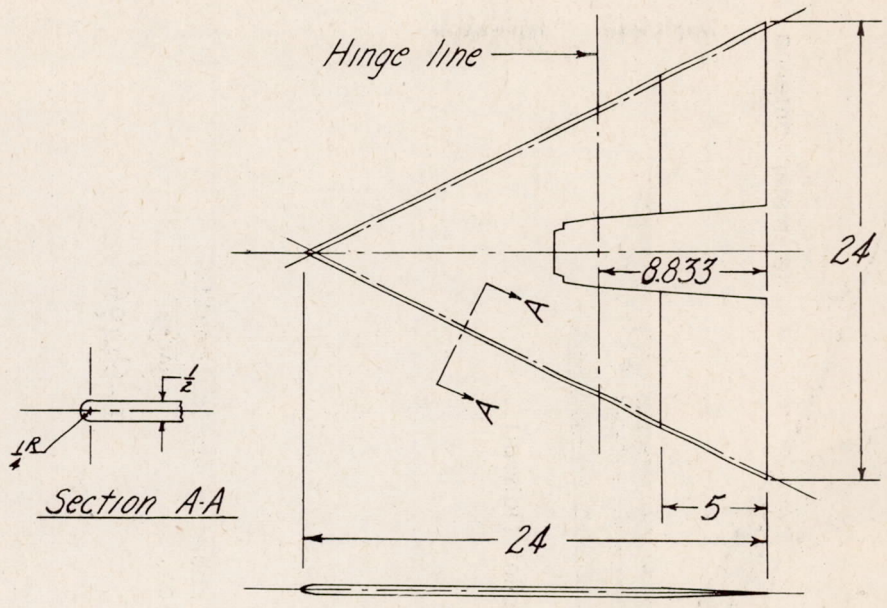
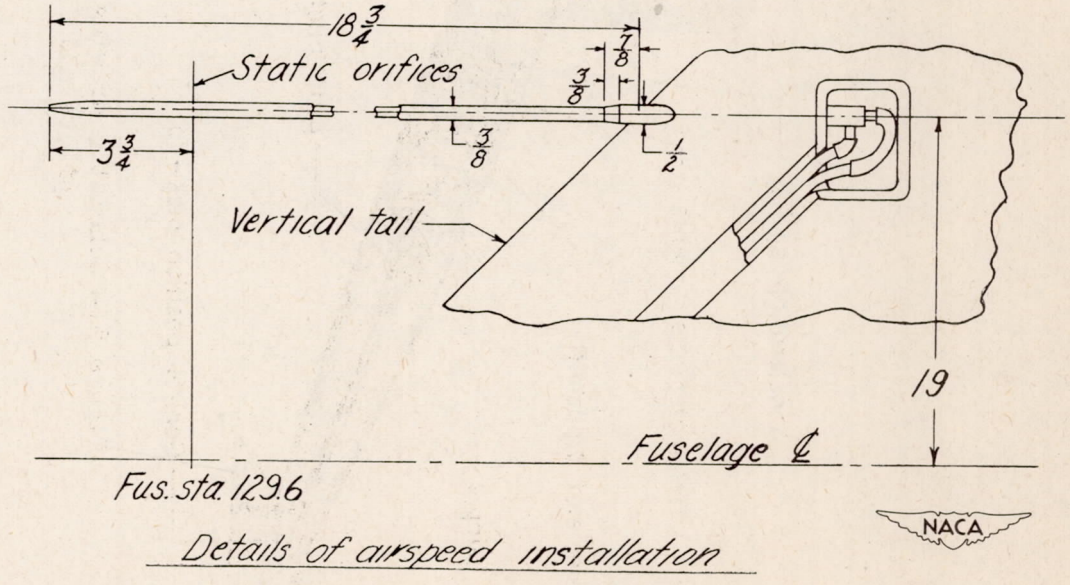


Figure 3.– Details of the tip of the wing and vertical tail of the canard model. All dimensions are in inches.



Details of horizontal control surface



Details of airspeed installation

Figure 4.– Details of the horizontal control surface and airspeed installation of the canard model. All dimensions are in inches.

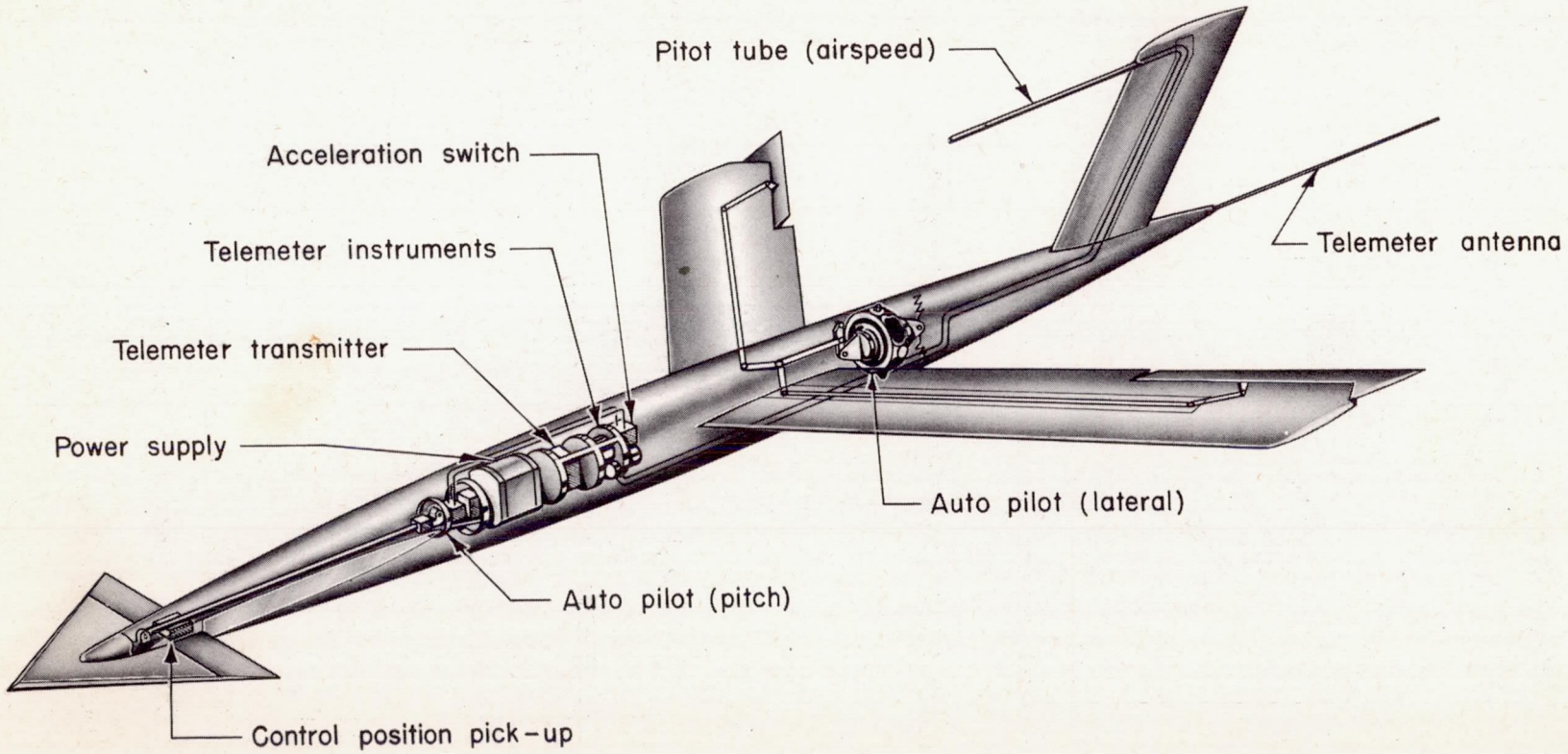


Figure 5.– Schematic drawing of the canard model showing the automatic pilots and internal instrumentation.

NACA

L-64496

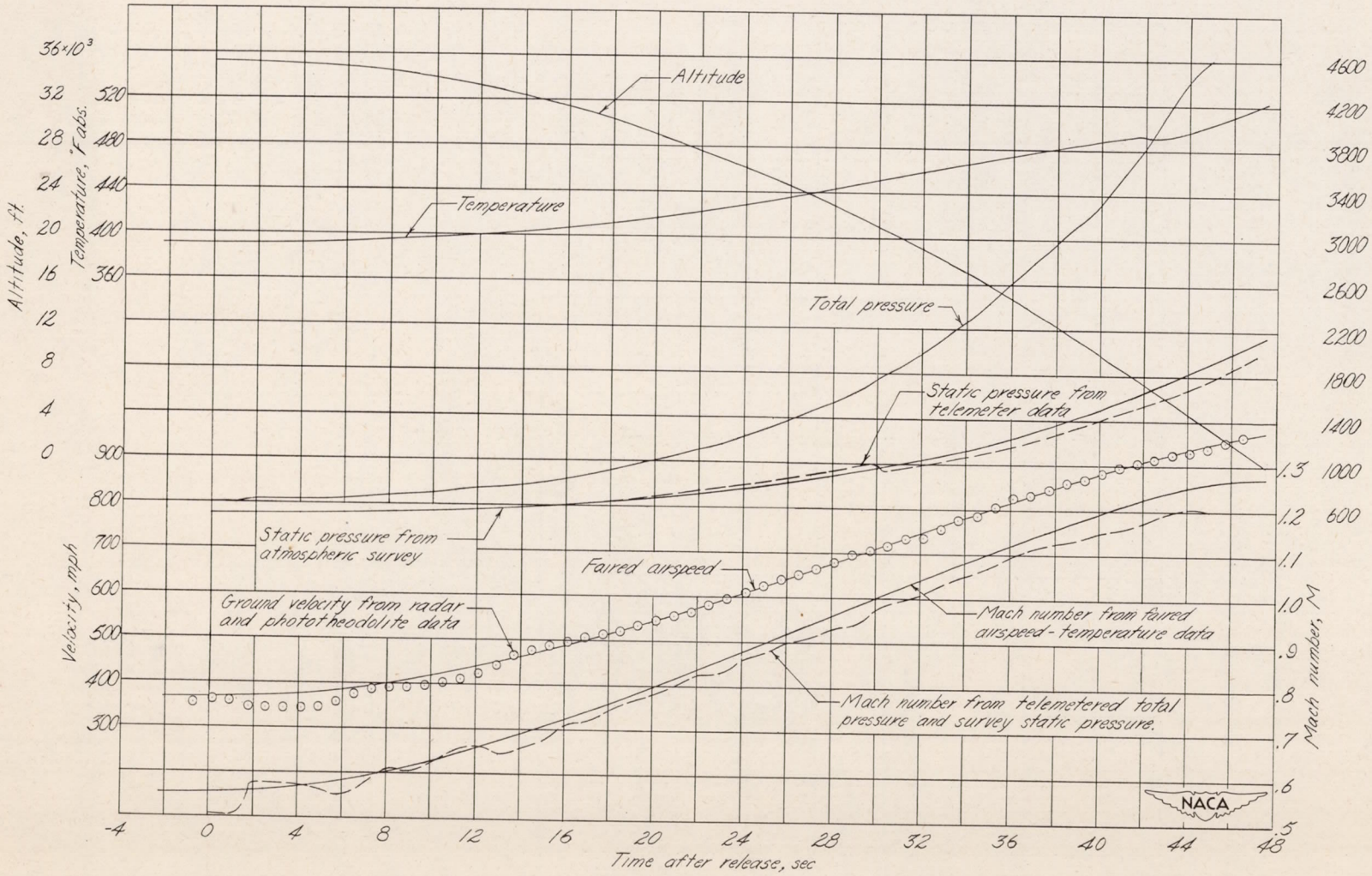


Figure 6.– Time histories of the measured quantities used in determining Mach number for the canard model test.

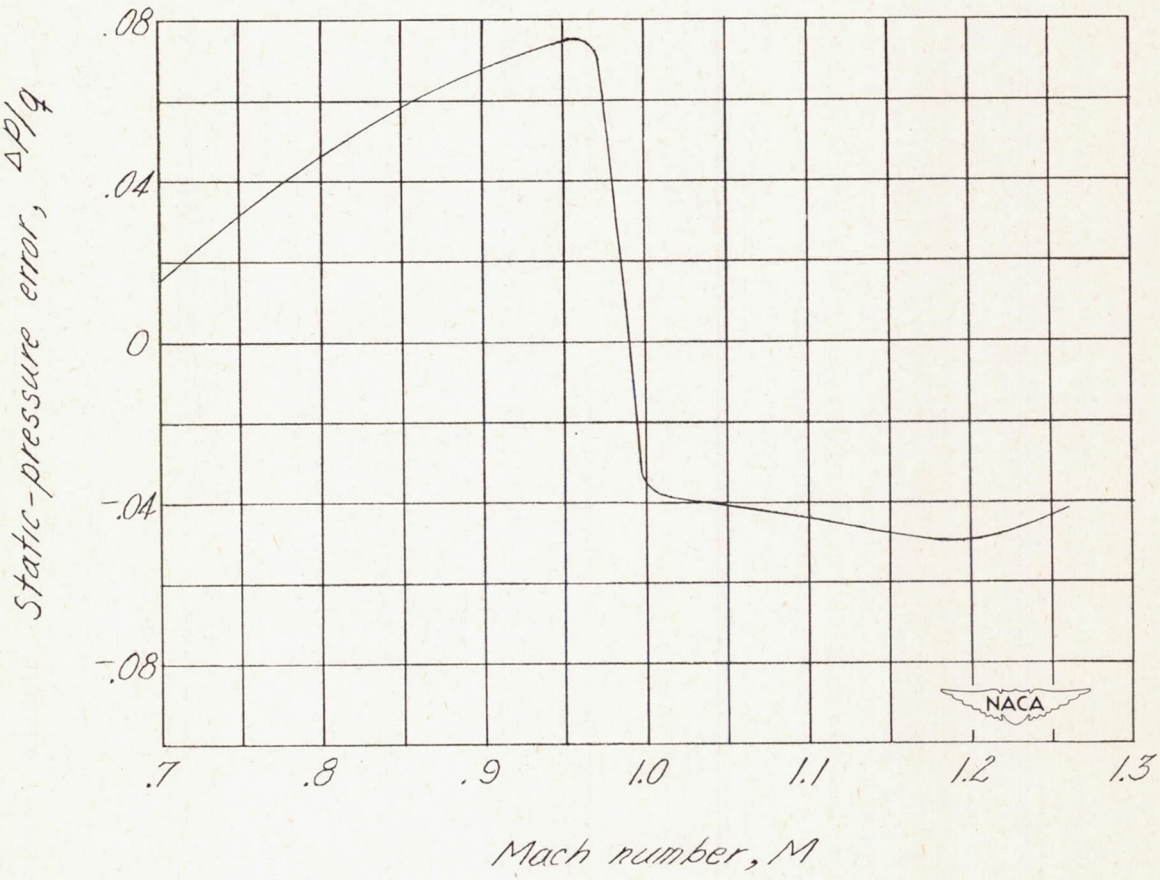


Figure 7.– Variation of the static–pressure error $\Delta p/q$ with Mach number for the airspeed head installation of the canard model.

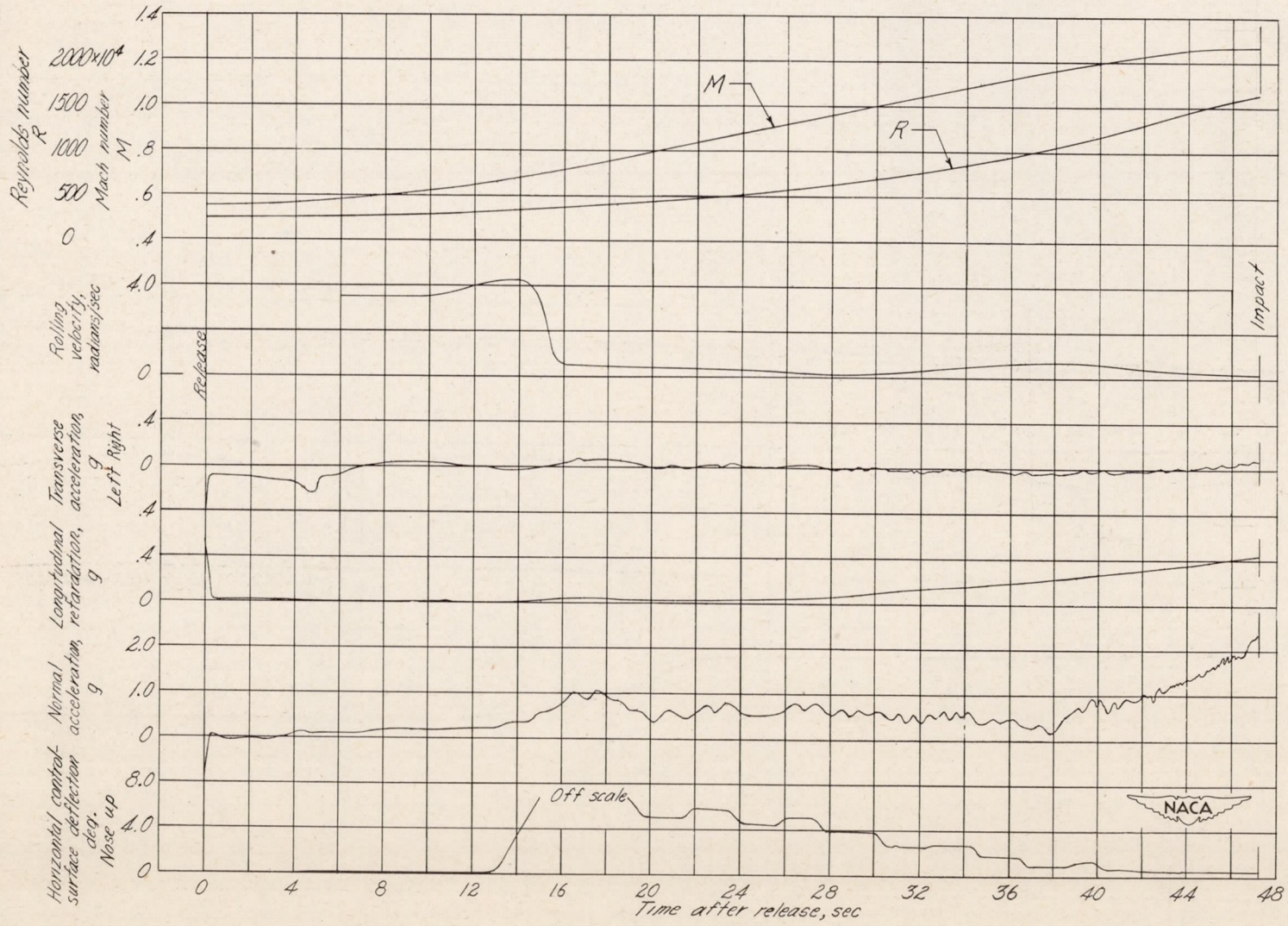


Figure 8.– Time history of the quantities measured during the free-fall of the canard model.

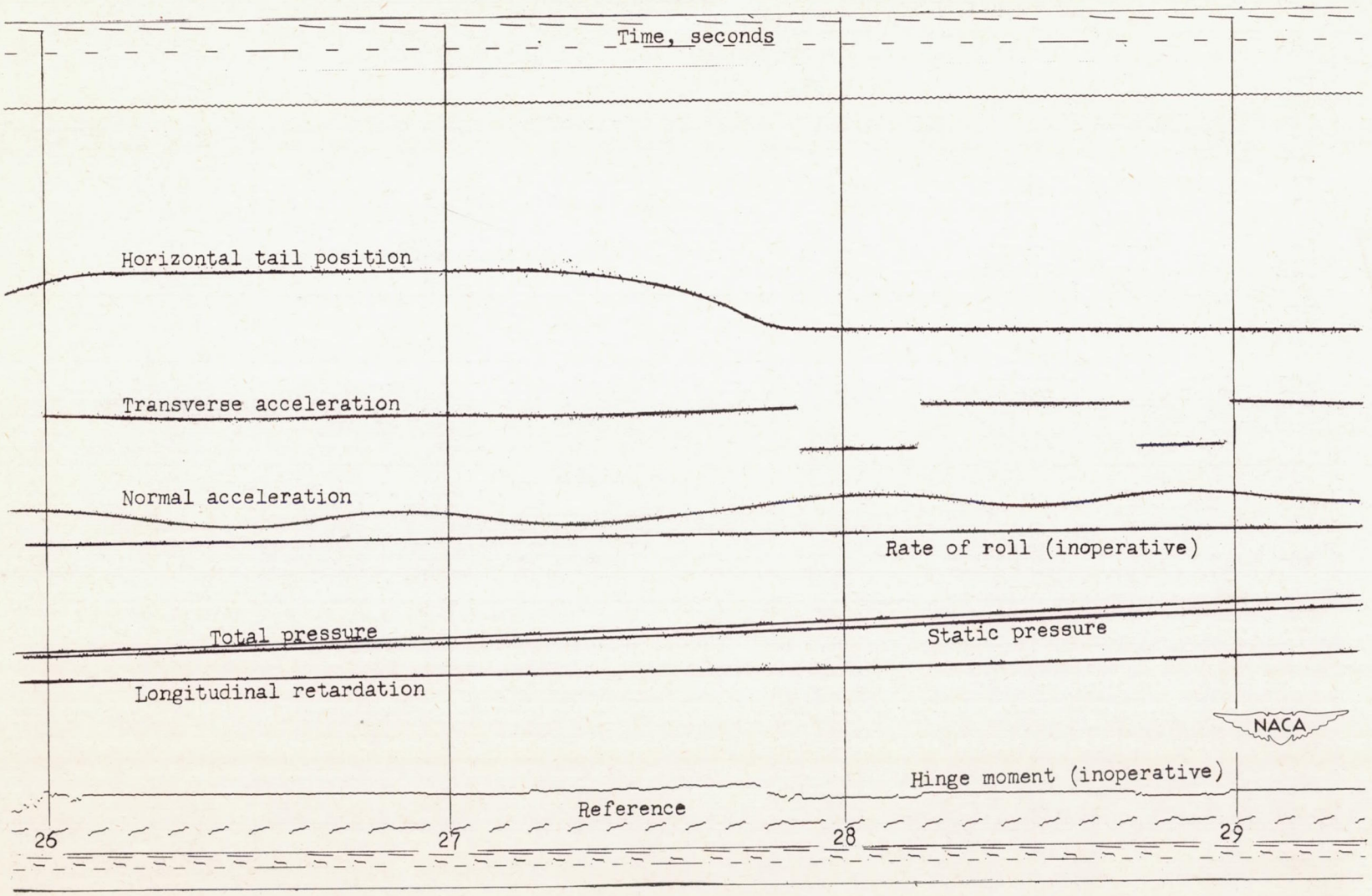


Figure 9.– A typical section of the telemeter record of the free-fall test of the canard model.

CONFIDENTIAL

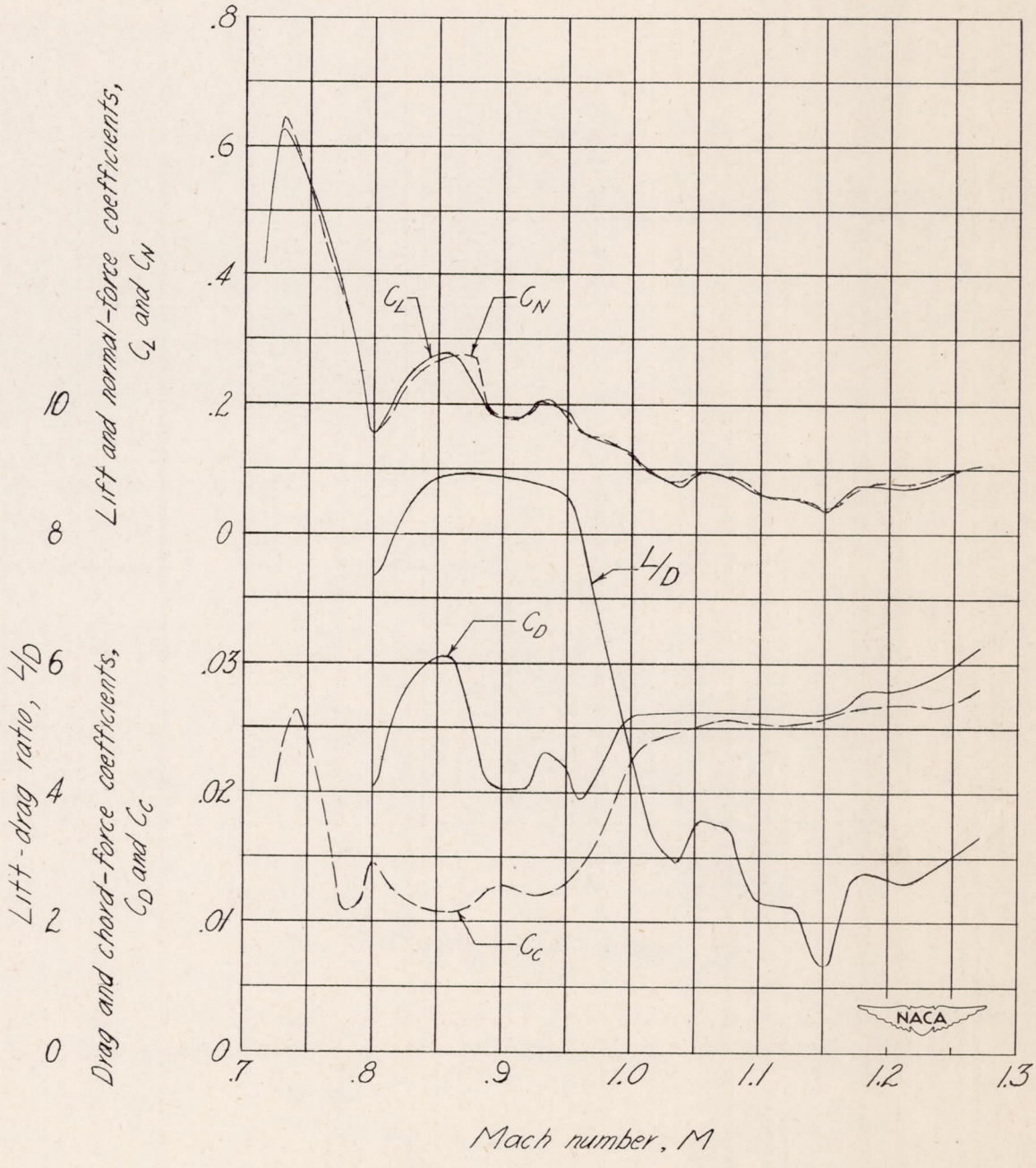


Figure 10.– Variation of the normal–force coefficient, lift coefficient, chord–force coefficient, drag coefficient, and lift–drag ratio as a function of Mach number for the canard model.

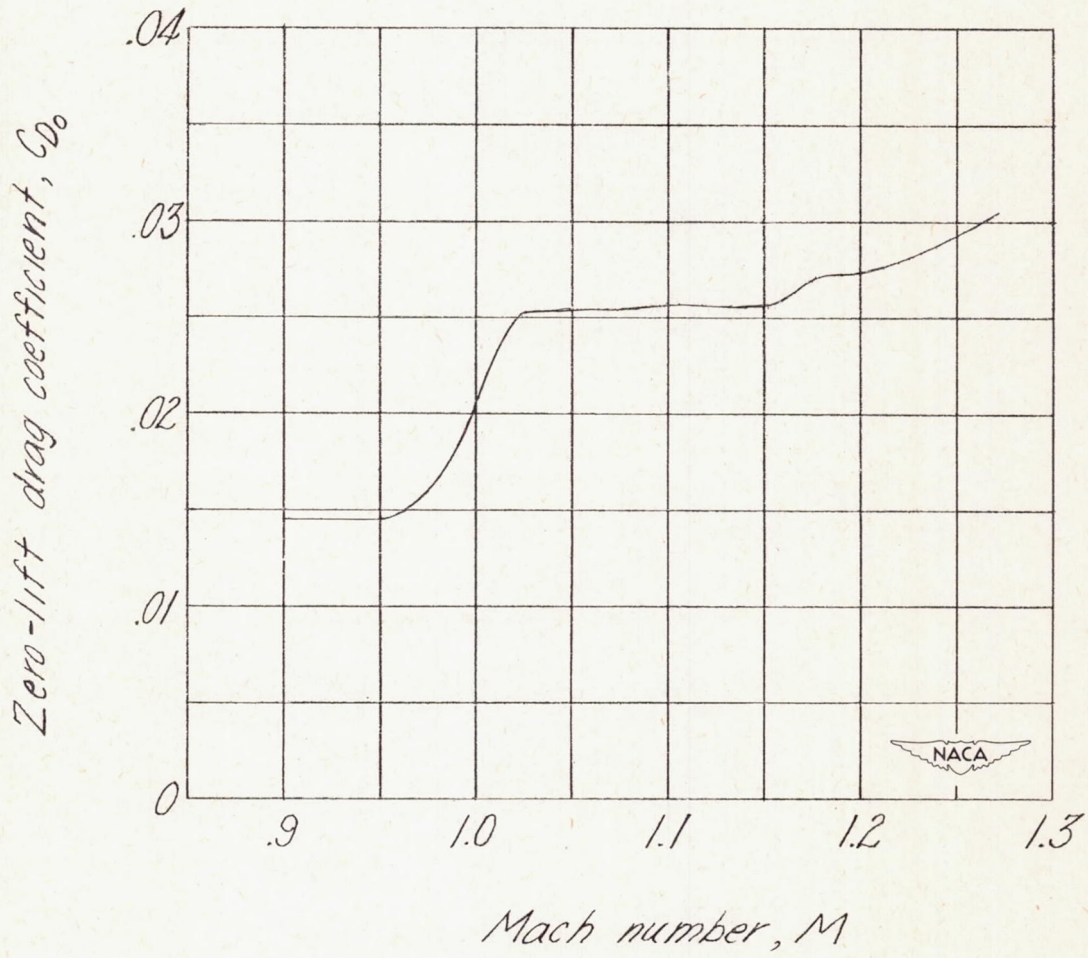


Figure 11.– Variation of the zero–lift drag coefficient as a function of Mach number based on the test data of the canard model.

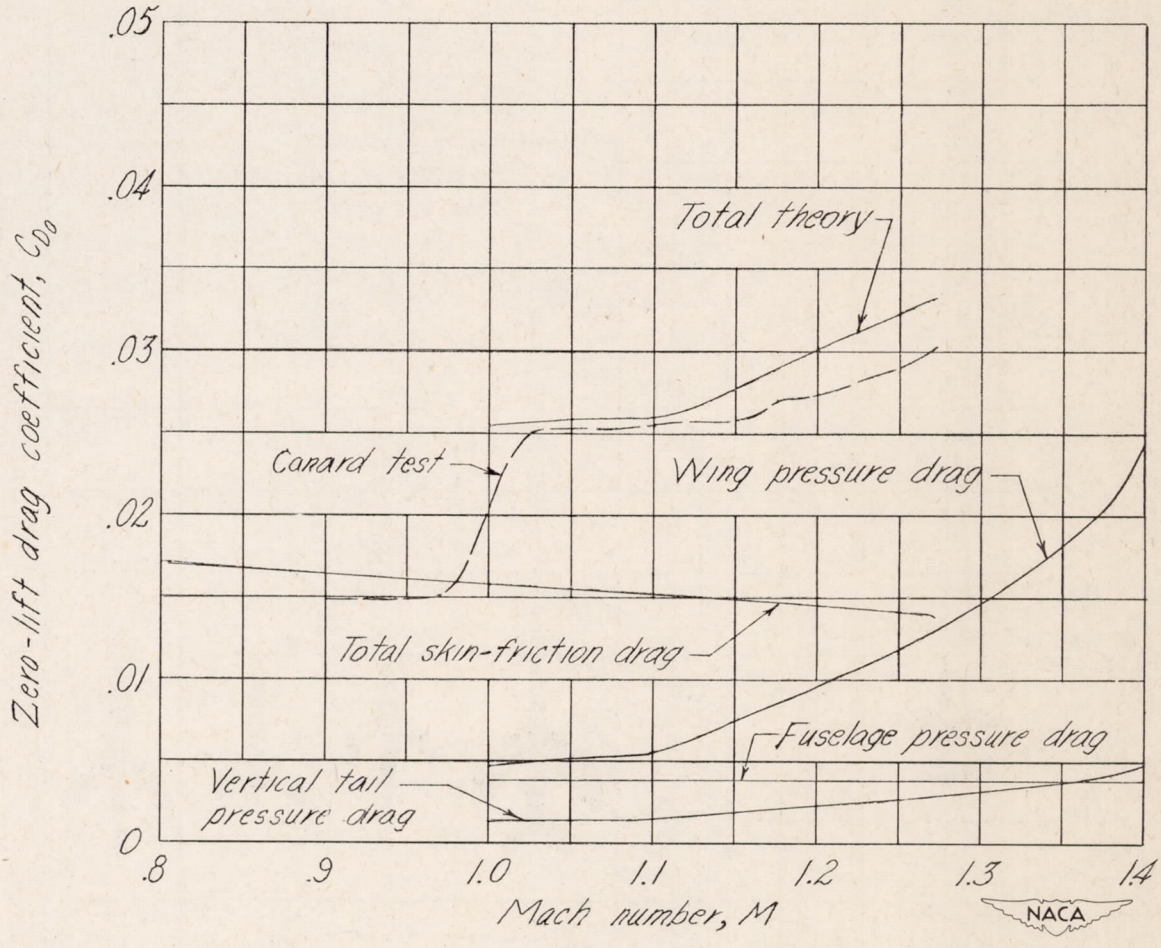


Figure 12.– Comparison of the zero–lift drag coefficients of the canard model with those predicted by supersonic theory.

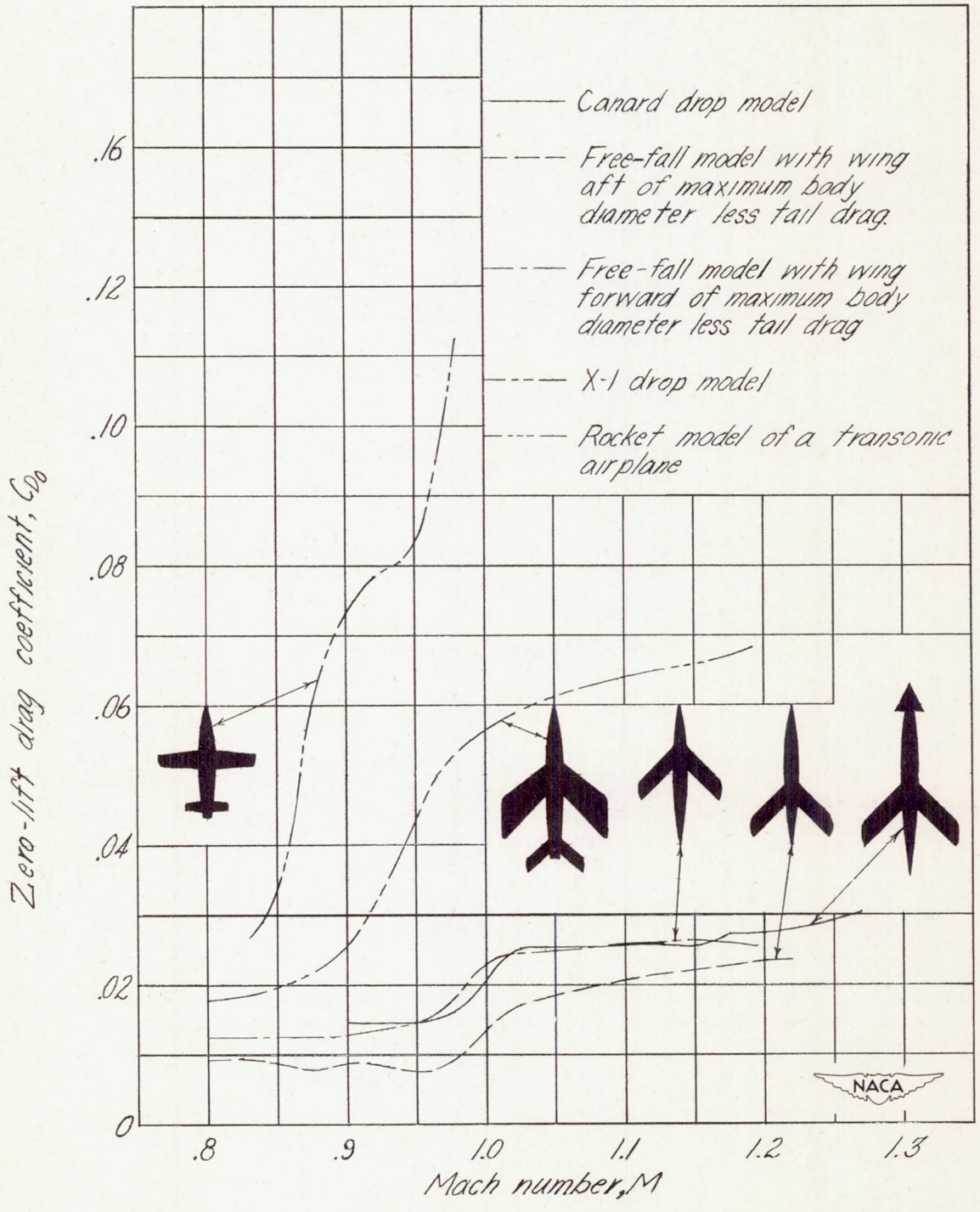


Figure 13.– Variation of the zero–lift drag coefficient with Mach number for the canard model and other transonic configurations. (The scale of the silhouettes has no significance.)

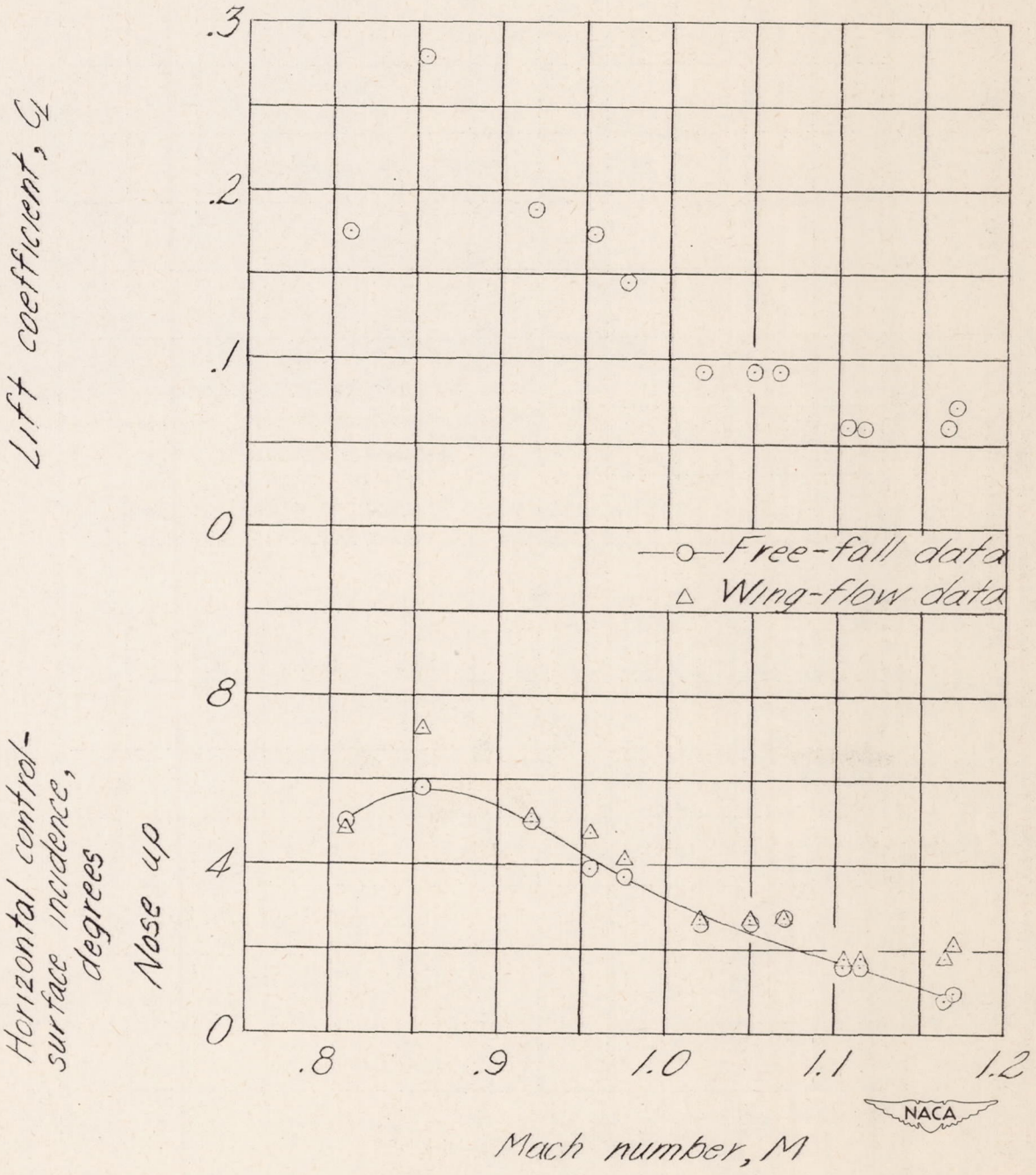


Figure 14.- Variation of the horizontal control-surface incidence required for trim as a function of Mach number for the canard model and for a similar canard model tested by the wing-flow method.

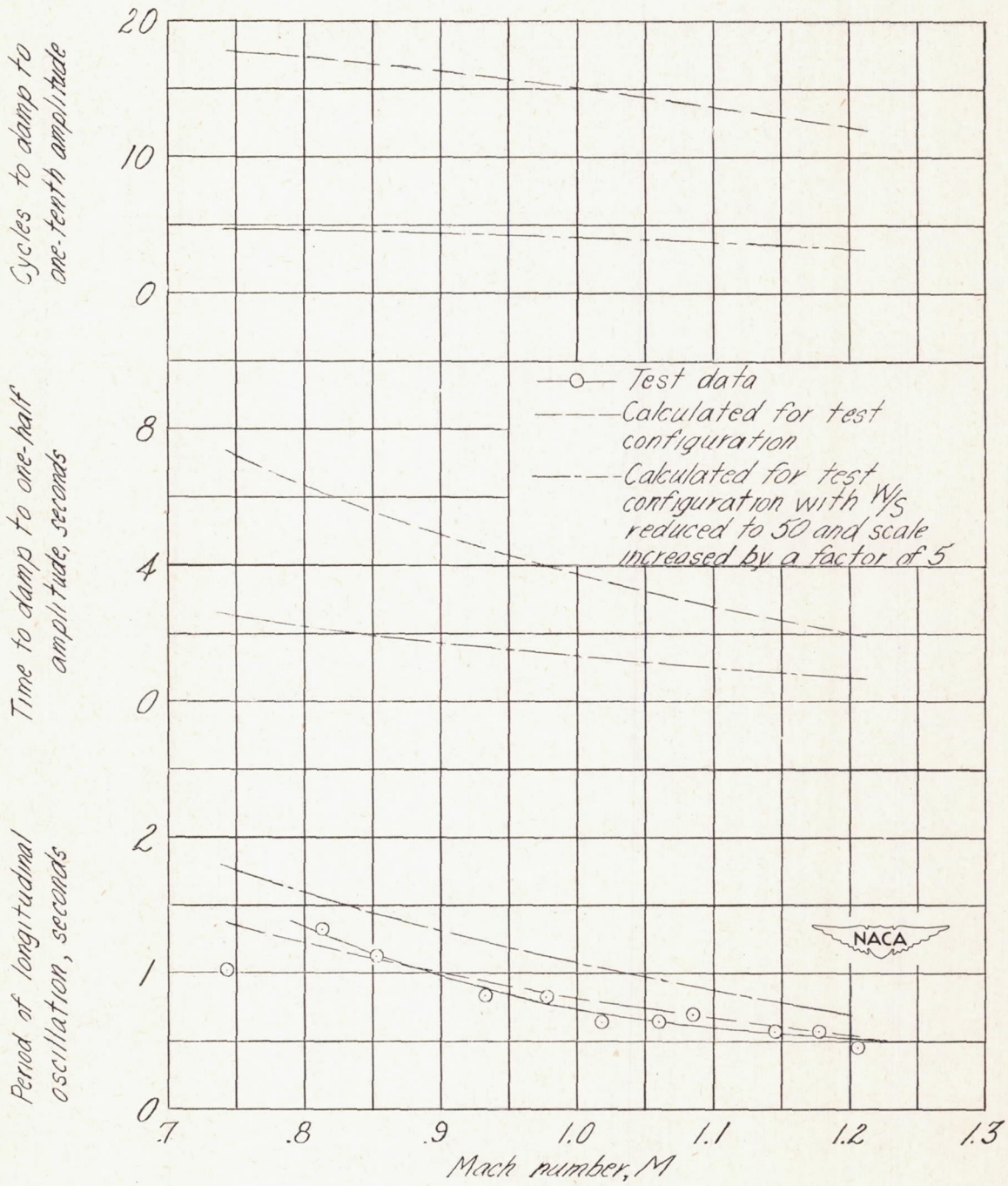


Figure 15.– Variation of the measured period and the calculated period and damping of the longitudinal oscillations as a function of Mach number for the canard model. (The calculated values shown include the same altitude variation as the test data.)

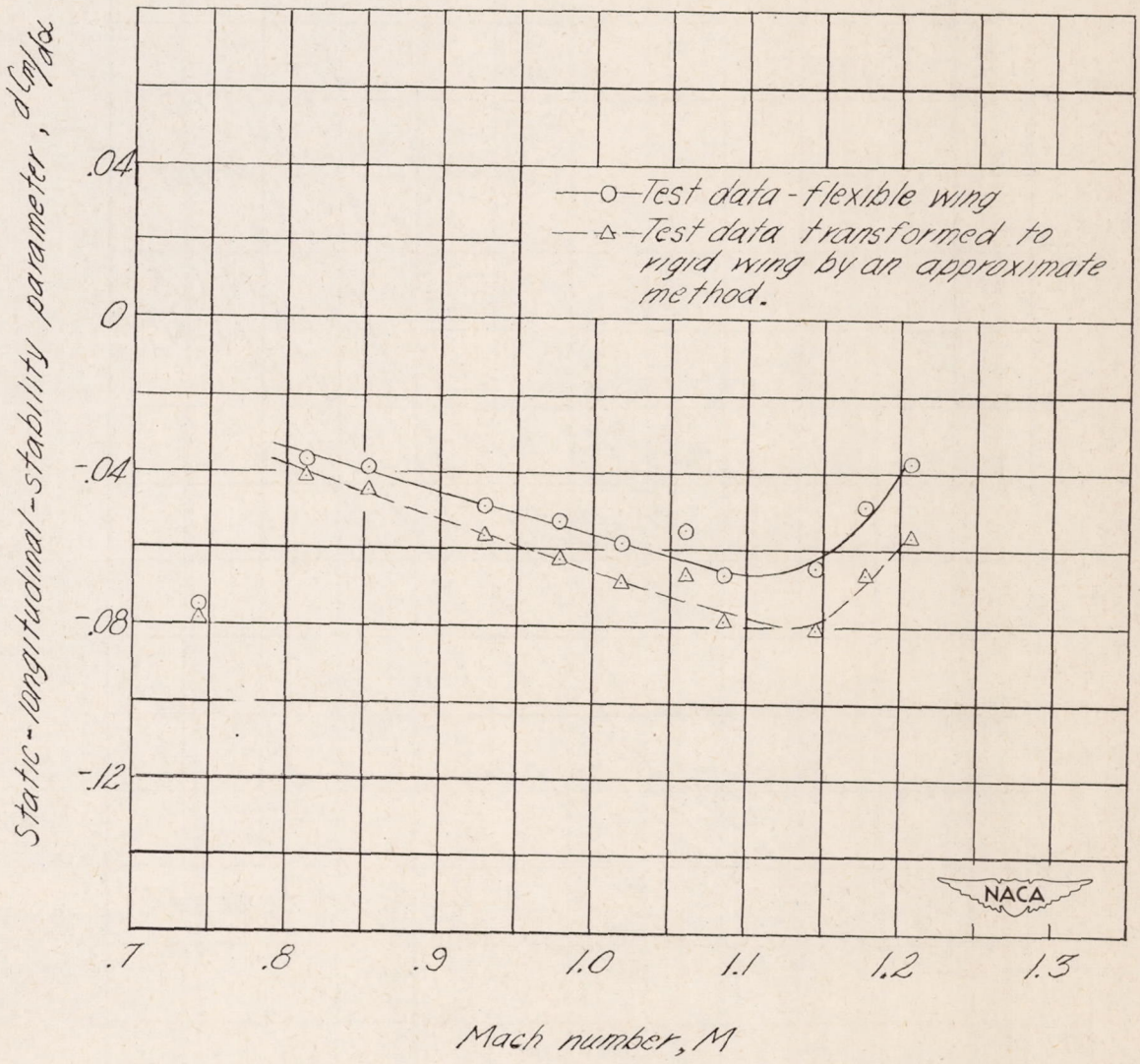


Figure 16.– Static–longitudinal–stability parameter $dC_m/d\alpha$ as a function of Mach number for the canard model.

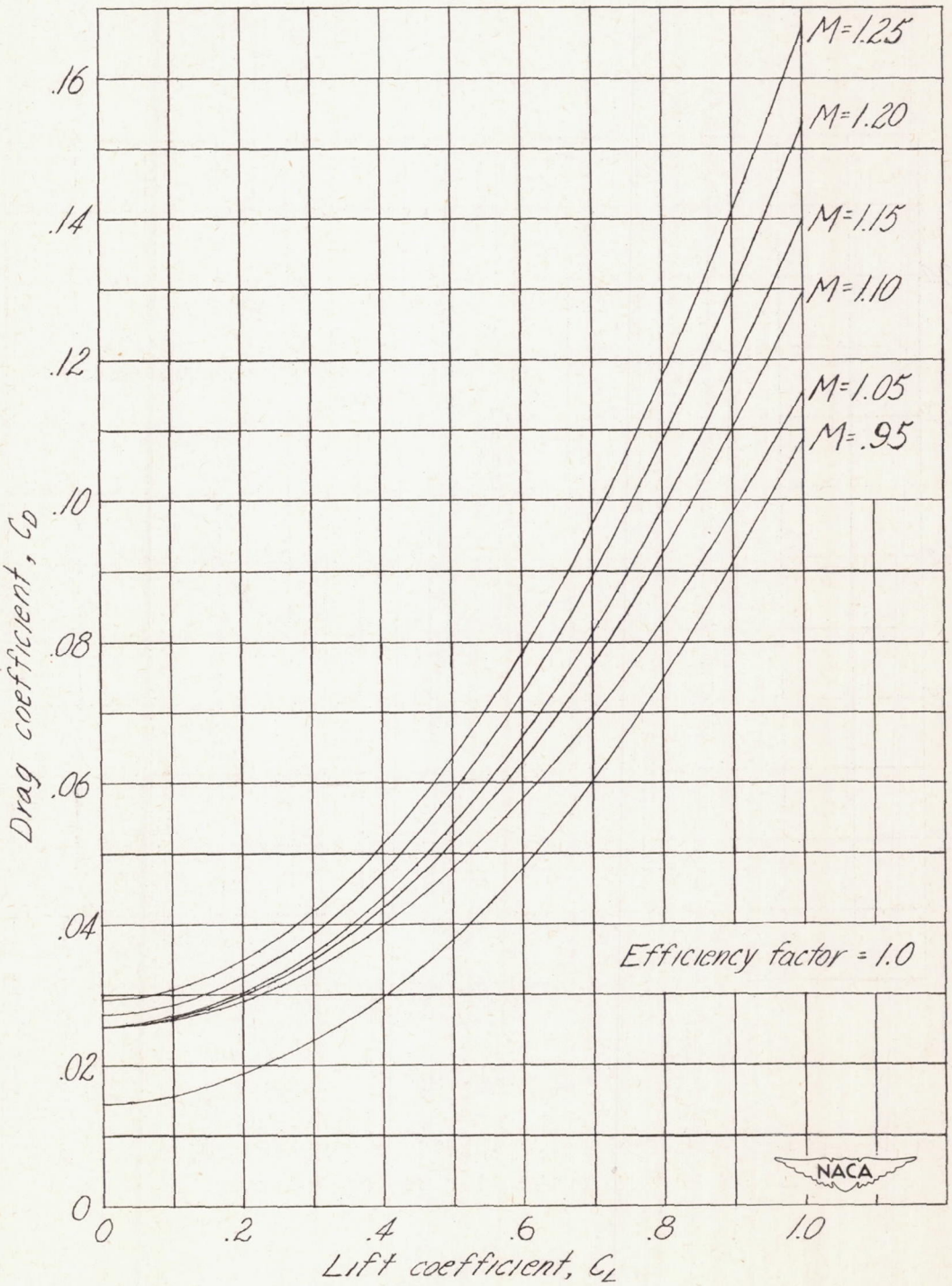


Figure 17.– Estimated lift–drag polars at various Mach numbers based on the zero–lift drag coefficients of the canard model. Control–surface incidence zero.

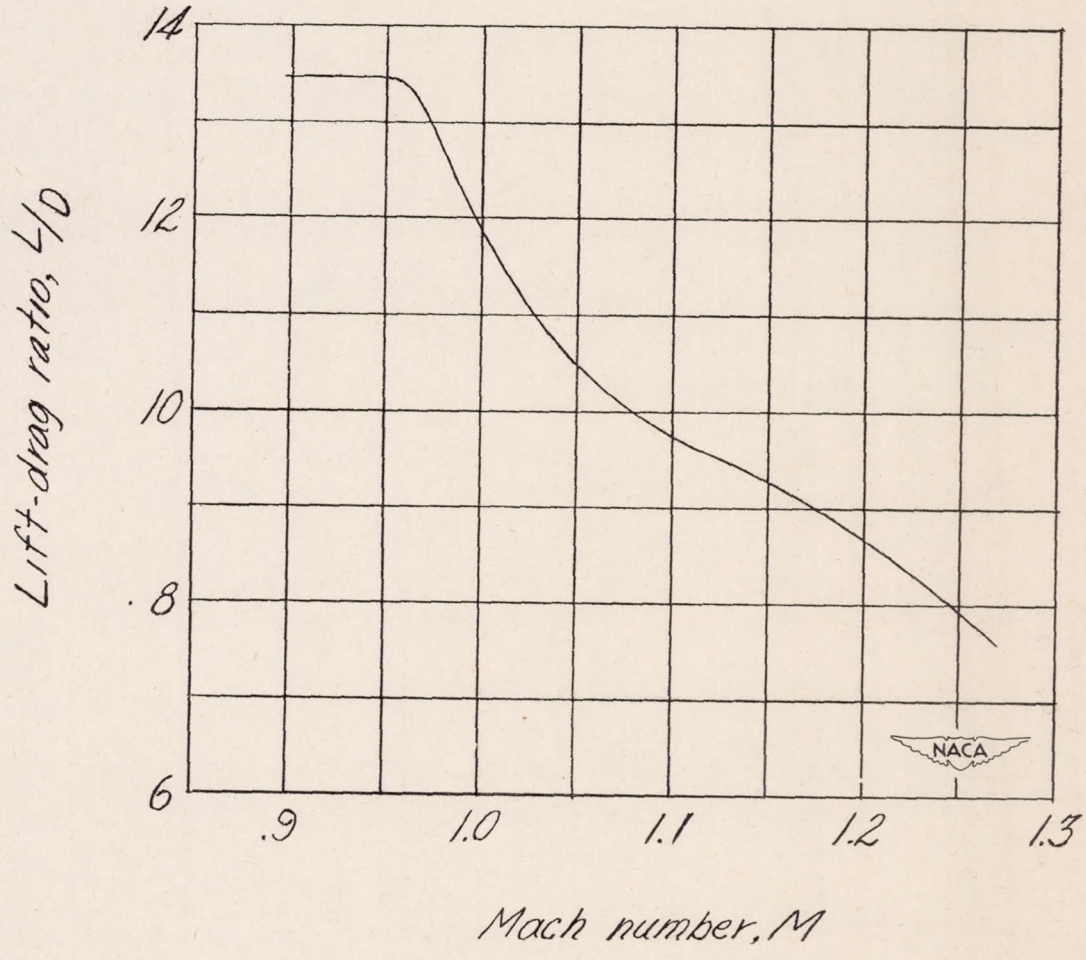


Figure 18.– Variation of the maximum lift–drag ratio with Mach number based on the lift–drag polars computed for the canard model. Control-surface incidence zero.

NACA-Langley - 8-25-50 - 350